Construction and Building Materials 236 (2020) 117417

Contents lists available at ScienceDirect

Construction and Building Materials

journal homepage: www.elsevier.com/locate/conbuildmat

Hyper-viscoelastic constitutive models for predicting the material behavior of polyurethane under varying strain rates and uniaxial tensile loading

H.M.C.C. Somarathna [a,b,*], S.N. Raman [b,c,*], D. Mohotti [d], A.A. Mutalib [b], K.H. Badri [e]

[a] Department of Civil Engineering, Faculty of Engineering, University of Jaffna, Ariviyal Nagar, Killinochchi 44000, Sri Lanka
[b] Smart and Sustainable Township Research Centre (SUTRA), Faculty of Engineering and Built Environment, Universiti Kebangsaan Malaysia, 43600 UKM Bangi, Selangor, Malaysia
[c] Centre for Innovative Architecture and Built Environment (SErAMBI), Faculty of Engineering and Built Environment, Universiti Kebangsaan Malaysia, 43600 UKM Bangi, Selangor, Malaysia
[d] Centre for Infrastructure Engineering, Western Sydney University, Penrith, NSW 2751, Australia
[e] Faculty of Science and Technology, Universiti Kebangsaan Malaysia, 43600 UKM Bangi, Selangor, Malaysia

HIGHLIGHTS

- A viscoelastic model was proposed to simulate variation in mechanical properties of elastomers.
- Hyper-viscoelastic constitutive models were developed to simulate mechanical behaviour of elastomers.
- The proposed models could be used to predict material behavior using model parameters.

GRAPHICAL ABSTRACT

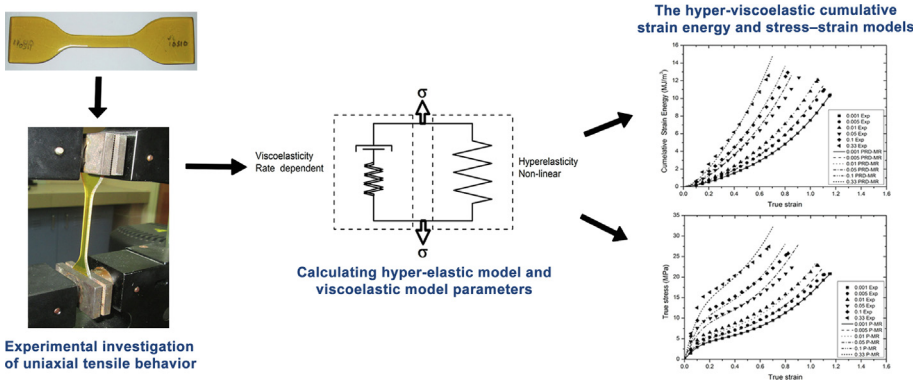

ARTICLE INFO

Article history:
Received 30 October 2018
Received in revised form 24 October 2019
Accepted 28 October 2019

Keywords:
Hyperelasticity
Viscoelasticity
Hyper-viscoelastic constitutive models
Polyurethane

ABSTRACT

Non-linearity, loading rate, as well as temperature and pressure dependency present major challenges in the investigation of properties, particularly the mechanical properties of elastomeric polymers. Recently, material and structural engineers have focused on investigating the mechanical behavior of hyper-elastic materials under varying strain rate conditions. In addition, they have been developing constitutive models to define the non-linear behavior of these materials, combined with the strain rate effect, which simulates behavior under different loading conditions. In this study, a new viscoelastic model is proposed to simulate the variation in the mechanical properties of elastomeric materials. Hyper-viscoelastic constitutive models were also developed by modifying existing hyper-elastic models (Mooney–Rivlin and Ogden) with existing viscoplastic models (Cowper–Symonds and Johnson–Cook) and the proposed viscoelastic model. The proposed models were verified through experimental results by investigating the uniaxial tensile behavior of an elastomeric polyurethane (PU) sample under varying low strain rate regimes ($0.001\ s^{-1}$–$0.1\ s^{-1}$). The proposed viscoelastic model exhibited the best correlation to present the enhancement of mechanical properties under varying strain rate conditions compared with the Cowper–Symonds and Johnson–Cook models. The proposed hyper-viscoelastic models could be used to

Abbreviations: DIF, Dynamic Increase Factor; FE, Finite Element; FEM, Finite Element Model; MDI, 4,4-diphenylmethane diisocyanate; PEG, Polyethylene glycol; PKO-p, Palm-based Polyol; PORCE, The Polymer Research Centre; PU, Polyurethane.

* Corresponding authors at: Faculty of Engineering and Built Environment, Universiti Kebangsaan Malaysia, 43600 UKM Bangi, Selangor, Malaysia.
E-mail addresses: hmccsomarathna@gmail.com (H.M.C.C. Somarathna), snraman@gmail.com (S.N. Raman).

https://doi.org/10.1016/j.conbuildmat.2019.117417

predict material behavior using only one set of hyper-elastic model parameters at a certain strain rate, combined with viscoelastic model parameters. The hyper-viscoelastic cumulative strain energy and stress–strain models, which were developed with the proposed viscoelastic model, demonstrated high accuracy in predicting material behavior with the strain rate effect of elastomeric PU or similar materials.

1. Introduction

Recent experimental and computational investigations on elastomeric polymer composites have highlighted positive contribution of elastomers in enhancing the performance of protective structures. Structures made out of construction materials such as metals, masonry, concrete, and other composites with elastomeric polymer coating have shown enhanced performance in their energy absorption capacity, permanent deformations, and fragmentation effect under dynamic loads [1–16]. Therefore, the behavior of elastomeric segmented copolymers under varying strain rates has gained significant attention at present because of the myriad of engineering, and battlefield applications designed with elastomeric polymer composites [17–33]. Their outstanding mechanical, thermal, and chemical properties, as well as self-healing capability, offer novel means to produce protective systems that are highly resilient yet dissipative [34–36]. The thermodynamic incompatibility and phase separation of soft and hard segmental copolymers in these elastomeric polymers result in hybrid mechanical properties, including several energy absorption and dissipation pathways [1,37–42]. In particular, the phase separation of soft and hard segments leads to a wide range of mechanical properties, ranging from soft to hard, which can be obtained by altering their chemical composition, molecular dispersion, additive and filler contents, as well as processing and synthesis techniques [1,6,37–42]. The properties of elastomers highly depend on several factors, such as temperature, pressure, and applied loading rate. Their loading rate-, temperature-, and pressure-dependent nonlinear behavior present major challenges in investigating the effect of these materials under dynamic applications [26–30]. Therefore, when investigating the mechanical behavior of elastomers, the deformation state and the working conditions must be considered to predict the behavior accurately.

The consistent and accurate quantitative characterization of mechanical properties is problematic in the field of material testing and more challenging under high strain rate conditions [17–24,26–33]. Given that the properties of elastomers are not linearly viscoelastic to large strains, using Boltzmann super positioning theory to deduce properties under high strain conditions is not well applicable [33]. Although the mechanical performance of elastomers under quasi-static conditions can be evaluated using several procedures, standard test methods to evaluate their dynamic response remain scarce because of the difficulty in maintaining homogeneous strain under high strain rate conditions [17,18]. Different test methods are available to investigate material properties experimentally under low to high strain rates, such as the universal test machine, the high-speed impact or the drop hammer testing system, the Hopkinson bar testing system, the special video-controlled tensile testing system, various servo-hydraulic testing systems, the Zwick screw drive mechanical tester, the Taylor impact tester, the dynamic tensile extrusion tester, and other types of modified high-speed test configurations [17–24,26–33]. Recently, numerical and computational investigations have been used frequently, and thus, several hyper-elastic constitutive models have been proposed to predict the non-linear behavior of these elastomeric polymers, such as Mooney–Rivlin [42,43] and Ogden [44]. Such hyper-elastic models are basically modeled using the strain energy density function in terms of strain invariants, which do not consider inelastic behavior. These constitutive models can define the stress–strain behavior of hyper-elastic materials using model parameters, which can be derived from simple experimental results [42–44]. However, these original hyper-elastic models are rate insensitive, and are commercially available advanced computer simulation codes, such as ANSYS ® [45] and LS-DYNA ® [46], are still using the original versions of such material models that are applicable under limited conditions. Therefore, including strain rate-dependent effects in original models is necessary to characterize behavior at different strain rates [22–24,34,47,48]. In addition, several viscoplastic constitutive models have been proposed to define the rate-dependent mechanical behavior of materials and have been used to modify hyper-elastic models by introducing viscoplastic models to account for constitutive contribution under varying strain rates [23,24,34,47,48]. These models will also be straightforward methods for obtaining accurate and cost-effective estimates.

Polyurethanes (PUs) are hyperelastic and viscoelastic materials, and synthesized from aromatic or aliphatic isocyanates with the chemical functionality of at least two hydroxyl groups [1,6]. The principal mechanical properties of PUs result from the segregation of hard segments within a soft phase. The hard domains consequently function as physical cross-links and generally lead to tough elastomers. The hard domains link the linear polymer chains in two directions, thereby forming a cross-linking network that governs elastic properties [37,38]. These elastomers are cross-linked by secondary valence bonding within the domains, such as hydrogen bonding, dipole interactions, and van der Waals interactions [39,40]. Although the dissociation energy of secondary valence interactions is less in magnitude by one or two orders than those of main valence bonds, such interactions provide an increase in cross-linking and controlling segmental mobility. Therefore, they provide higher thermal and mechanical stability compared with the stability of conventional cross-linking with only main valence bonding [39,40]. Molecular segregation is mainly promoted in PU because of the hydrogen bond formation among urethane linkages in different hard segments.

In this study, several hyper-viscoelastic constitutive models were developed by modifying existing hyper-elastic models by incorporating existing viscoplastic models. Their accuracy in predicting rate-dependent and non-linear behavior was evaluated through the experimental results, which were undertaken on an elastomeric PU sample under varying strain rates (0.001–0.33 s^{-1}) in a subsequent study, and recently reported experimental results by Mohotti et al. [23].

2. Constitutive models

2.1. Viscoplastic models

Viscoplastic models are used to define the material behavior under varying strain rates. The dynamic increase factor (DIF) is used to quantify enhancement in material properties under high strain rates, compared with the material properties under

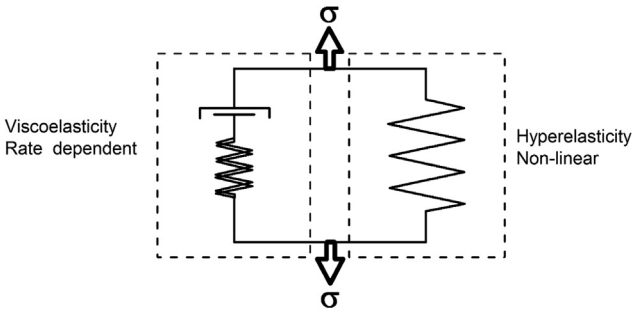

Fig. 1. Parallel mechanical response of viscoelasticity and hyperelasticity.

reference strain rate condition. Two selected viscoplastic models and one proposed model are as follows;

2.1.1. Cowper-Symonds model

The Cowper–Symonds model is a constitutive model that can be formulated to illustrate the DIF of a material property at high strain rates [22]. The Cowper–Symonds model is defined with two coefficients, as follows:

$$\mathrm{DIF} = 1 + \left(\frac{\dot{\varepsilon}}{D}\right)^{\frac{1}{q}} \tag{1}$$

where $\dot{\varepsilon}$ is the actual strain rate tested, and D and q are the Cowper–Symonds model coefficients. These coefficients can be determined by rearranging the preceding equation and then plotting and fitting the data of ln $\dot{\varepsilon}$ versus ln (DIF-1) linearly. The gradient of the linear correlation provides the coefficient q, and the intercept represents ln D. The original Cowper–Symonds model could not represent the dynamic effect of material properties, which are inversely correlated with strain rate. Therefore, the Cowper–Symonds model was modified as follows:

$$\frac{1}{\mathrm{DIF}} = 1 + \left(\frac{\dot{\varepsilon}}{D}\right)^{\frac{1}{q}} \tag{2}$$

where $\dot{\varepsilon}$ is the actual strain rate tested, and D and q are the Cowper–Symonds model coefficients.

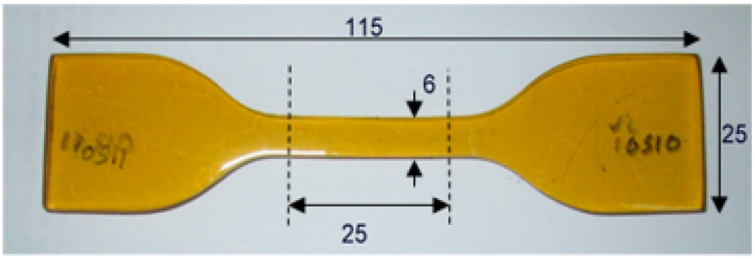

(a)

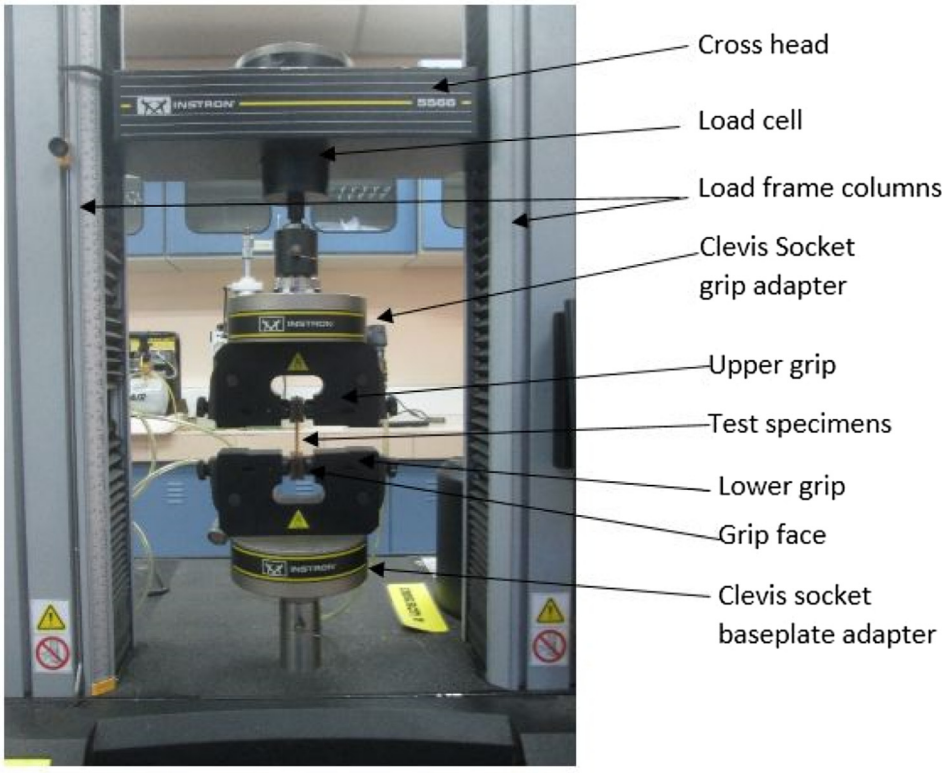

(b)

Fig. 2. The: (a) Tensile test specimen (Dimensions in mm); and (b) Uniaxial tensile test setup [6].

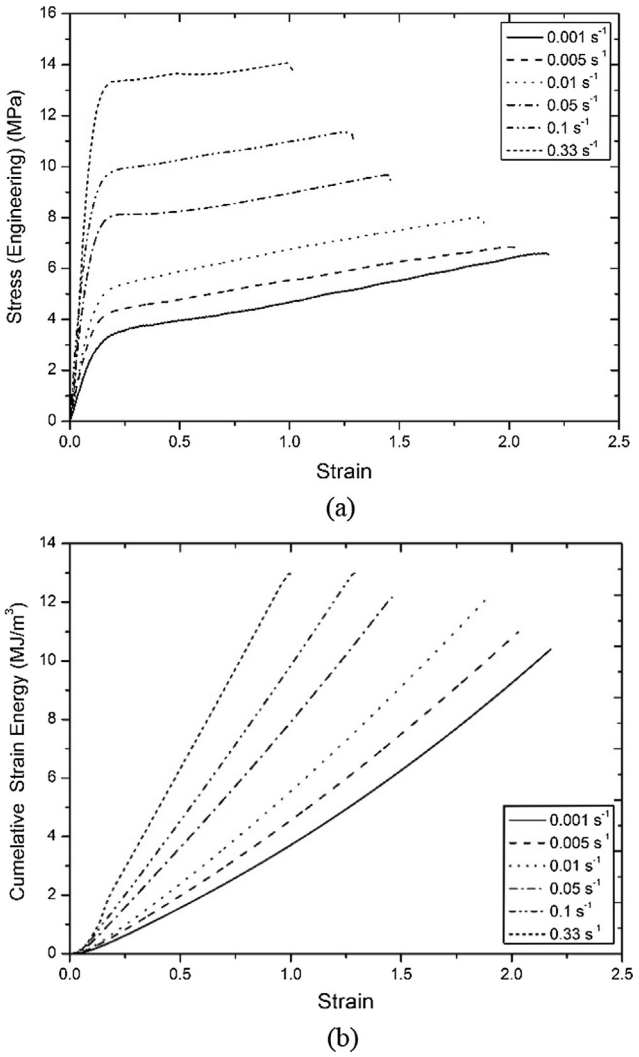

Fig. 3. (a) Engineering stress–strain; and (b) cumulative strain energy of PU sample under varying strain rates.

2.1.2. Johnson-Cook model

The Johnson–Cook constitutive model (1983) is a phenomenological model that is used to reproduce the responses of several materials, particularly metals [49,50]. This model includes three key material responses: strain hardening, strain rate dependency, and thermal softening. These responses are combined in a multiplicative manner. In this study, only the strain rate-dependent material response is used, which is as follows:

$$\mathrm{DIF} = 1 + C\ln\dot{\varepsilon}^{*} \tag{3}$$

where C is the strain rate parameter, $\dot{\varepsilon}^{*}$ is the normalized strain rate that is defined as $\dot{\varepsilon}^{*} = \frac{\dot{\varepsilon}}{\dot{\varepsilon}_0}$, $\dot{\varepsilon}$ is the actual strain rate tested, and $\dot{\varepsilon}_0$ is the reference strain rate. The stranded strain rate-dependent Johnson–Cook model provides a linear relationship with the logarithm of normalized strain rate. The coefficient C can be determined by rearranging the preceding equation and then plotting and fitting the data of (DIF-1) versus ln $\dot{\varepsilon}^{*}$ linearly through the origin. The gradient of the linear correlation gives the coefficient C.

2.1.3. Proposed model

Another constitutive model is proposed by the authors in this study by observing the limitations in both Cowper–Symonds and Johnson–Cook models. The initial investigations show that the Cowper–Symonds model is not well representative at high strain levels and yields overestimated values. Moreover, the actual enhancement in material properties does not linearly vary with the logarithm of normalized strain rate as in the Johnson–Cook model. Accordingly, the proposed constitutive model is formulated to illustrate the DIF of a material property at varying strain rates compared with the material properties under reference strain rate condition as follows:

$$\mathrm{DIF} = 1 + \frac{1}{A}\left(\ln\dot{\varepsilon}^{*}\right)^{B} \text{ when } \dot{\varepsilon} > \dot{\varepsilon}_0, \text{ and DIF} = 1 \text{ when } \dot{\varepsilon} < \dot{\varepsilon}_0 \tag{4}$$

where A and B are the strain rate parameters, and $\dot{\varepsilon}^{*}$ is the normalized strain rate that is defined in the same manner as that in the Johnson–Cook model. These coefficients can be determined by rearranging the preceding equation and then plotting and fitting the data of ln $(\ln\dot{\varepsilon}^{*})$ versus ln (DIF-1) linearly. The gradient of the linear correlation provides the coefficient B, and the intercept represents ln A.

In addition, some material properties, such as failure strain and tangent modulus, are demonstrated to be reduced with strain rate. To represent the behavior of material properties that are reduced with strain rate, the proposed model is modified as follows:

$$\frac{1}{\mathrm{DIF}} = 1 + \frac{1}{A}\left(\ln\dot{\varepsilon}^{*}\right)^{B} \text{ when } \dot{\varepsilon} > \dot{\varepsilon}_0, \text{ and DIF} = 1 \text{ when } \dot{\varepsilon} < \dot{\varepsilon}_0 \tag{5}$$

The coefficients can be determined by plotting and fitting the data of ln $(\ln\dot{\varepsilon}^{*})$ versus ln $(\frac{1}{\mathrm{DIF}})$ linearly.

2.2. Hyperelastic material models

Elastomeric materials exhibit rate dependency in terms of energy absorption and strength. The use of elastomeric materials to enhance the dynamic resistance of structures has recently been demonstrated in both research and applications. These materials undergo varying strain rates, including high strain rates during complex dynamic events, such as blast and ballistic impacts. Empirical models are used to analyze their behavior in both numerical and analytical investigations, including in FE codes. The Mooney–Rivlin and Ogden models are widely used and encoded in ANSYS ® [45] and LS-DYNA ® [46] software, which are rate-insensitive.

Table 1
Tensile characteristics at different strain levels.

Strain rate (s^{-1})	Young's modulus (MPa)	Yield stress (MPa)	Tangent modulus (MPa)	Ultimate stress (MPa)	Failure stress (MPa)	Failure strain	Resilience modulus (MJm^{-3})	Toughness modulus (MJm^{-3})
0.001	22.61	3.34	1.69	6.63	5.98	2.19	0.22	9.99
0.005	30.76	4.41	1.55	7.16	6.55	2.02	0.32	11.07
0.01	35.06	5.28	1.49	7.75	7.26	1.86	0.34	11.69
0.05	55.69	7.94	1.55	9.80	9.14	1.50	0.63	12.52
0.1	71.83	9.81	1.47	11.32	10.99	1.27	0.69	12.68
0.33	93.45	12.96	0.63	13.88	13.34	1.04	0.75	13.12

Table 2
The coefficients of each viscoplastic and viscoelastic models for the DIF of each tensile material property.

Material property	Cowper-Symonds model		Johnson-Cook model	Proposed model	
	D	q	C	A	B
Young's modulus	0.0298	1.8418	0.4582	6.9261	1.7383
Yield stress	0.0299	2.0951	0.4584	7.1621	1.7112
Tangent modulus	0.2751	1.3804	−0.0634	32.4273	1.5391
Ultimate stress	0.2232	1.6664	0.1504	37.6638	2.1156
Failure stress	0.1640	1.6778	0.1778	24.2811	1.9416
Failure strain	0.2170	1.6961	−0.0852	32.4630	2.0326
Resilience modulus	0.0268	2.1748	0.4116	5.2028	1.5012
Toughness modulus	3.2269	6.4553	0.0591	12.6645	0.8130

2.2.1. Mooney-Rivlin model

The Mooney–Rivlin model has exhibited high accuracy in predicting the non-linear behavior of isotropic elastomeric materials [43,44]. This model is currently used in considerable research and finite element (FE) codes as a constitutive model to characterize the behavior of hyper-elastic materials. The original Mooney–Rivlin model is rate-insensitive and is limited to predicting the behavior at a given strain level or in conditions under which the strain rate effect is insignificant. To predict the behavior at varying strain rates, the Mooney–Rivlin parameters for each strain level should be determined individually using the curve-fitting method. The Mooney–Rivlin model applies to the solid, shell, beam, and plane elements of present technologies [23,43,44].

$$W = \psi(\bar{I}_1, \bar{I}_2, J) = \sum_{i,r=0}^{n} C_{ir}\left(\bar{I}_1 - 3\right)^i \left(\bar{I}_2 - 3\right)^r + \sum D_k (J-1)^{2k} \quad (6)$$

where W is the strain energy potential; C_{ir} is the material constant related to the deviatoric deformation of the material; $\bar{I}_1$ and $\bar{I}_2$ are the first and second strain invariants of the left Cauchy–Green deformation tensor, respectively; C_{10} and C_{01} are the characterizations of the material constants; and D_k is the material constant related to the incompressibility response. $\bar{I}_1$ and $\bar{I}_2$ can be explained as follows:

$$\bar{I}_1 = J^{-2/3} I_1;\ I_1 = \lambda_1^2 + \lambda_2^2 + \lambda_3^2 \quad (7)$$

$$\bar{I}_2 = J^{-4/3} I_2;\ I_2 = \lambda_1^2\lambda_2^2 + \lambda_2^2\lambda_3^2 + \lambda_3^2\lambda_1^2 \quad (8)$$

where λ_k, $k = 1, 2, 3$ are the principal stretches by considering the constant volume requires,

$$\lambda_1\lambda_2\lambda_3 = 1 \quad (9)$$

The simplest model for a compressible material is given with two parameters, and the strain energy potential is expressed in terms of three material parameters as follows,

$$W = C_{10}\left(\bar{I}_1 - 3\right) + C_{01}\left(\bar{I}_2 - 3\right) + D_1(J-1)^2 \quad (10)$$

Although the two-parameter Mooney–Rivlin model is widely used, its accuracy is limited because it does not provide an accurate strain energy density at high stretches. Therefore, the Mooney–Rivlin model has been further modified by several researchers, and few other versions of the Mooney–Rivlin model are currently used as the three-, five-, and nine-parameter models. These models provide a good representation of the behavior at high stretches, and they have been used in the FE codes ANSYS ® [45] and LS-DYNA ® [46].

For 3 parameters, the strain energy potential is formed as:

$$W = C_{10}\left(\bar{I}_1 - 3\right) + C_{01}\left(\bar{I}_2 - 3\right) + C_{11}\left(\bar{I}_1 - 3\right)\left(\bar{I}_2 - 3\right) + D_1(J-1)^2 \quad (11)$$

For 5 parameter, the strain energy potential is formed as:

$$W = C_{10}\left(\bar{I}_1 - 3\right) + C_{01}\left(\bar{I}_2 - 3\right) + C_{11}\left(\bar{I}_1 - 3\right)\left(\bar{I}_2 - 3\right) + C_{20}\left(\bar{I}_1 - 3\right)^2 + C_{02}\left(\bar{I}_2 - 3\right)^2 + D_1(J-1)^2 \quad (12)$$

For 9 parameter, the strain energy potential is formed as:

$$W = C_{10}\left(\bar{I}_1 - 3\right) + C_{01}\left(\bar{I}_2 - 3\right) + C_{11}\left(\bar{I}_1 - 3\right)\left(\bar{I}_2 - 3\right) + C_{20}\left(\bar{I}_1 - 3\right)^2 + C_{02}\left(\bar{I}_2 - 3\right)^2 + C_{21}\left(\bar{I}_1 - 3\right)^2\left(\bar{I}_2 - 3\right) + C_{12}\left(\bar{I}_1 - 3\right)\left(\bar{I}_2 - 3\right)^2 + C_{30}\left(\bar{I}_1 - 3\right)^3 + C_{03}\left(\bar{I}_2 - 3\right)^3 + D_1(J-1)^2 \quad (13)$$

where C_{10}, C_{01}, C_{11}, C_{20}, C_{02}, C_{21}, C_{12}, C_{30}, C_{03} and D_1 are the material constants.

In this study, the nine-parameter strain energy potential is used because of its high accuracy. From Eqns. (7) and (8), for incompressible materials $J = 1$ and under uniaxial tension $\lambda = \lambda_1$ and $\lambda_2 = \lambda_3 = 1/\sqrt{\lambda_1} = 1/\sqrt{\lambda}$, we can further simplify this potential as follows.

$$W = C_{10}(I_1 - 3) + C_{01}(I_2 - 3) + C_{11}(I_1 - 3)(I_2 - 3) + C_{20}(I_1 - 3)^2 + C_{02}(I_2 - 3)^2 + C_{21}(I_1 - 3)^2(I_2 - 3) + C_{12}(I_1 - 3)(I_2 - 3)^2 + C_{30}(I_1 - 3)^3 + C_{03}(I_2 - 3)^3 + D_1(J-1)^2 \quad (14)$$

Correspondingly, the Cauchy (true) stress can be derived as follows in terms of two strain invariants:

$$\sigma = 2(\lambda^2 - \frac{1}{\lambda})(\frac{\partial\psi}{\partial\bar{I}_1} + \frac{1}{\lambda}\frac{\partial\psi}{\partial\bar{I}_2}) \quad (15)$$

2.2.2. Ogden model

The Ogden model is another model that is frequently used to predict the behavior of hyper-elastic materials [44].

$$W = \sum_{i=1}^{N} \frac{\mu_i}{\alpha_i}(\bar{\lambda}_1^{\alpha_i} + \bar{\lambda}_2^{\alpha_i} + \bar{\lambda}_3^{\alpha_i} - 3) + \sum \frac{1}{d_k}(J-1)^{2k} \quad (16)$$

where W is the strain energy potential; $\bar{\lambda}_k^{\alpha_i}$ (k = 1, 2, 3) are the deviatoric principal stretches, defined as $\bar{\lambda}_k = J^{-\frac{1}{3}}\lambda_k$, λ_k (k = 1, 2, 3) are the principal stretches of the left Cauchy–Green tensor; J is the determinant of the elastic deformation gradient; and N, $\mu_k\alpha_k$, and d_k are the material constants

The N value has no limitation, and a good fit to the actual material behavior can be obtained with a high N value. However, considering the numerical difficulties in finding the material constants, extremely high N values are not used in practice. Therefore, 1, 2, and 3 are used as N values in research and FE codes. For

N = 2, $\alpha_1 = 2$, and $\alpha_2 = -2$, the Ogden model is the same as the two-parameter Mooney–Rivlin model.

The Ogden material constants are as follows. For N = 1: μ_1, α_1, d_1; for N = 2: μ_1, α_1, μ_2, α_2, d_1, d_2; for N = 3: μ_1, α_1, μ_2, α_2, μ_3, α_3, d_1, d_2, d_3; and for N = k: μ_1, α_1, μ_2, α_2, …, μ_k, α_k, d_1, d_2, …, d_k. For incompressible materials, $J = 1$. Under uniaxial tension, $\lambda = \lambda_1$ and $\lambda_2 = \lambda_3 = 1/\sqrt{\lambda_1} = 1/\sqrt{\lambda}$. Thus, this model can be further simplified as follows:

$$W = \sum_{i=1}^{N} \frac{\mu_i}{\alpha_i}\left(\lambda^{\alpha_i} + \frac{2}{\lambda^{\alpha_i/2}} - 3\right) \tag{17}$$

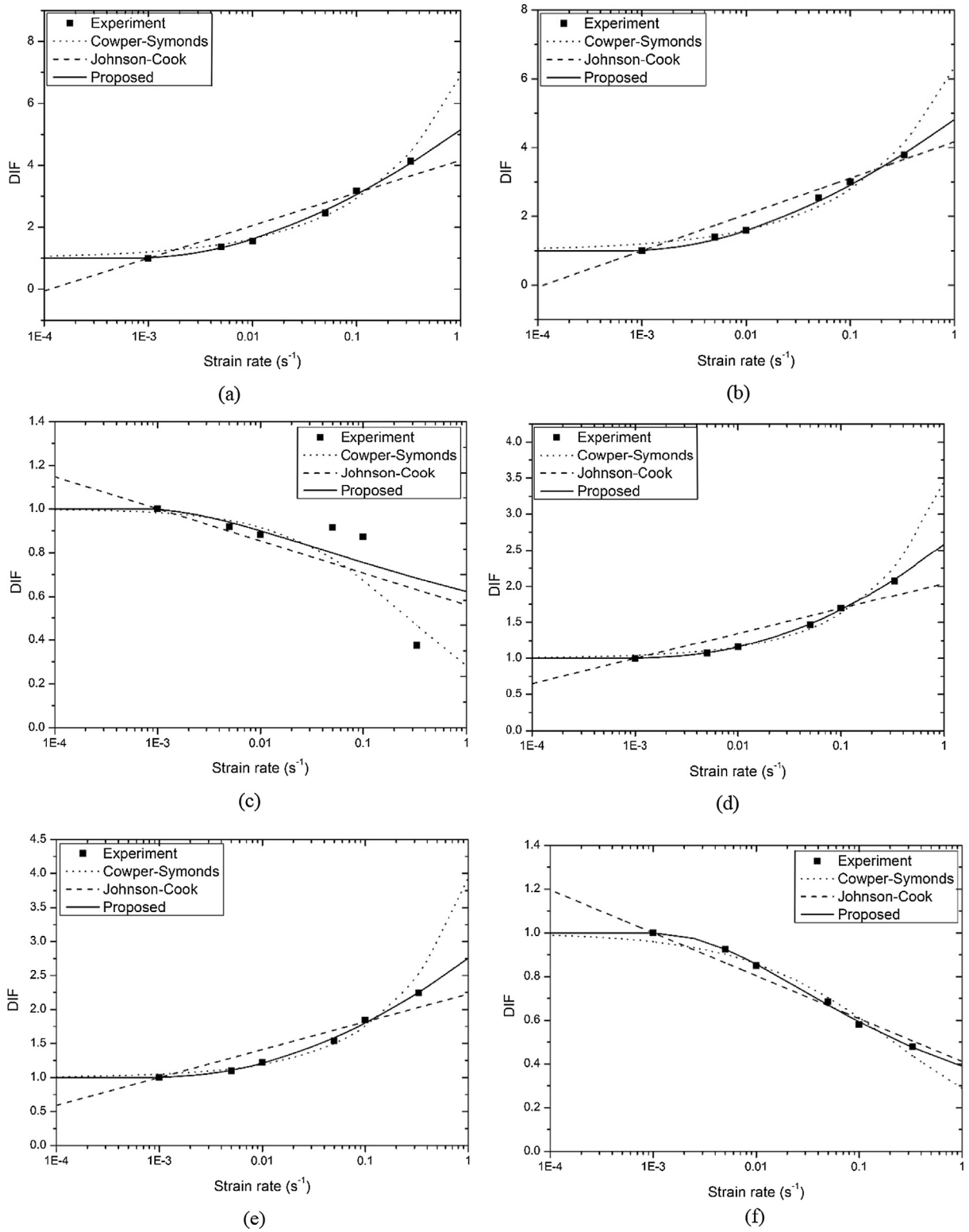

Fig. 4. DIF for tensile characteristic of PU at varying strain rates and the curve fit of the proposed DIF model; (a) Young's modulus; (b) Yield stress; (c) Tangent modulus; (d) Ultimate tensile stress; (e) Failure stress; (f) Failure strain; (g) Resilience modulus; (h) Toughness modulus.

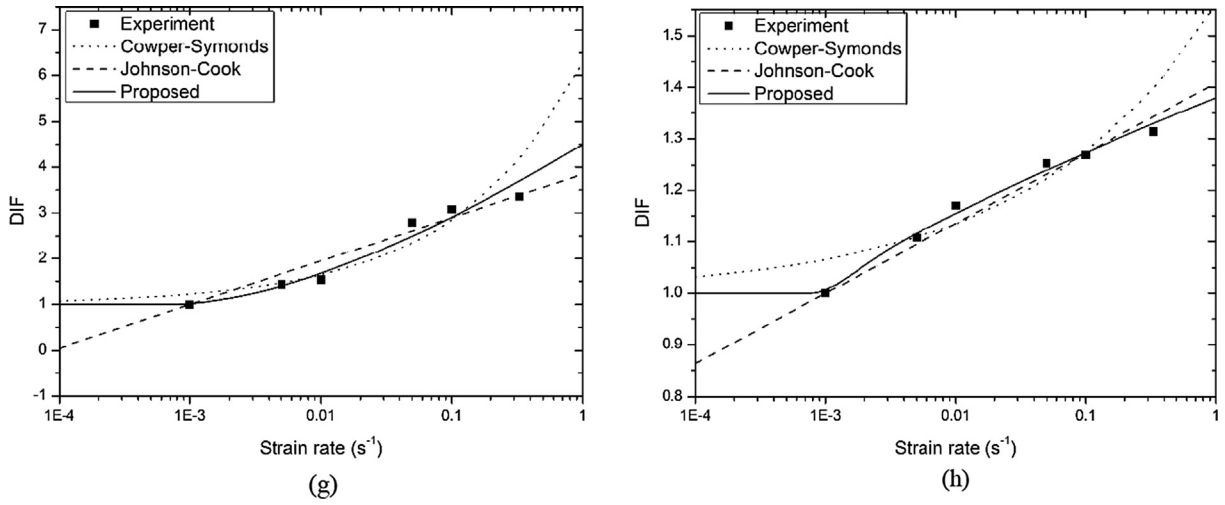

Fig. 4 (*continued*)

Table 3
The coefficient of determination, R^2, obtained for each tensile property.

Material property	Cowper-Symonds model	Johnson-Cook model	Proposed model
Young's modulus	0.9842	0.8990	0.9920
Yield stress	0.9690	0.9093	0.9991
Tangent modulus	0.6827	0.5273	0.4353
Ultimate stress	0.9697	0.8613	0.9995
Failure stress	0.9837	0.8783	0.9968
Failure strain	0.9773	0.9612	0.9978
Resilience modulus	0.9493	0.9411	0.9540
Toughness modulus	0.9365	0.9615	0.9734

In this study, three-parameter strain energy potential is used because of its high accuracy, and the energy potential is as follows.

$$W = \frac{\mu_1}{\alpha_1}(\lambda^{\alpha_1} + \frac{2}{\lambda^{\alpha_i/2}} - 3) + \frac{\mu_2}{\alpha_2}(\lambda^{\alpha_2} + \frac{2}{\lambda^{\alpha_2/2}} - 3) + \frac{\mu_3}{\alpha_3}(\lambda^{\alpha_3} + \frac{2}{\lambda^{\alpha_3/2}} - 3) \quad (18)$$

Correspondingly, the Cauchy (true) stress can be derived as follows.

$$\sigma = \frac{\partial W}{\partial \lambda} = \sum_{i=1}^{N} \mu_i \left(\lambda^{\alpha_i - 1} + \frac{2}{\lambda^{\frac{\alpha_i}{2}+1}} - 3 \right) \quad (19)$$

2.3. Hyper-viscoelastic material behaviour – energy models

Use of strain rate-insensitive constitutive models in predicting materials behavior in dynamic situations are inaccurate. Therefore, these hyper-elastic models should be modified into formats that can accurately predict material behavior together with strain rate effects. In this study, the original Mooney–Rivlin and Ogden models are improved by adding a strain rate-dependent term, which will be useful in reducing computation times and enhancing the accuracy of the models. Hyper-viscoelastic models are built by including two parallel material responses, namely, hyper-elasticity and strain rate dependency, which are combined in a multiplicative manner [Fig. 1]. The modified strain rate-sensitive Mooney–Rivlin and Ogden models are as follows.

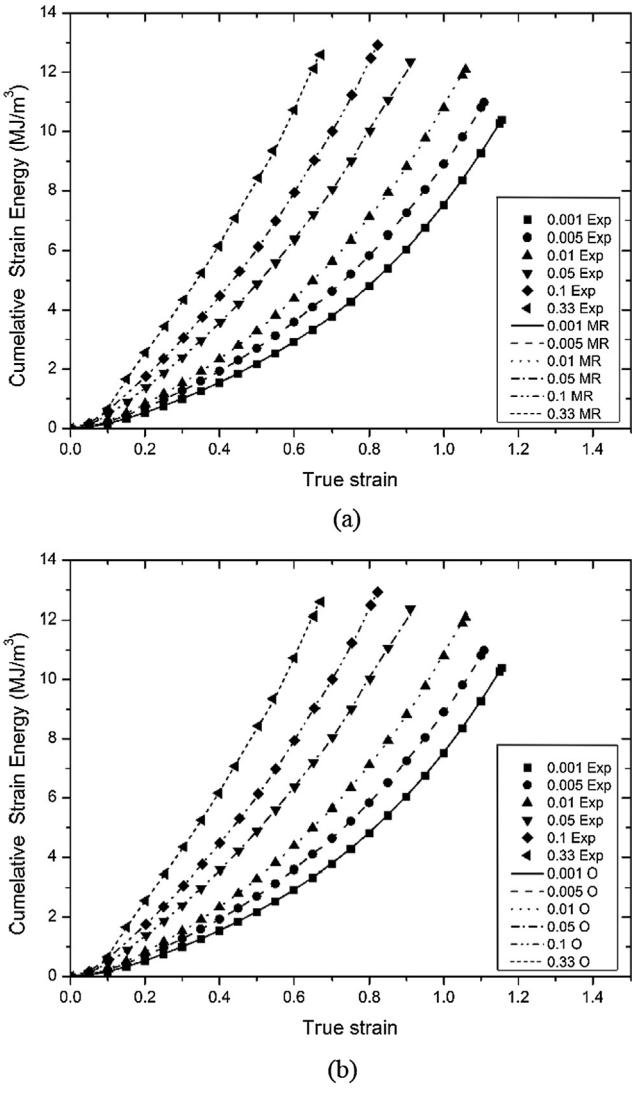

Fig. 5. Comparison of original hyperelastic model with experimental data to predict the cumulative strain energy of the PU sample (a) Nine-parameter Mooney-Rivlin; and (b) Three-parameter Ogden models.

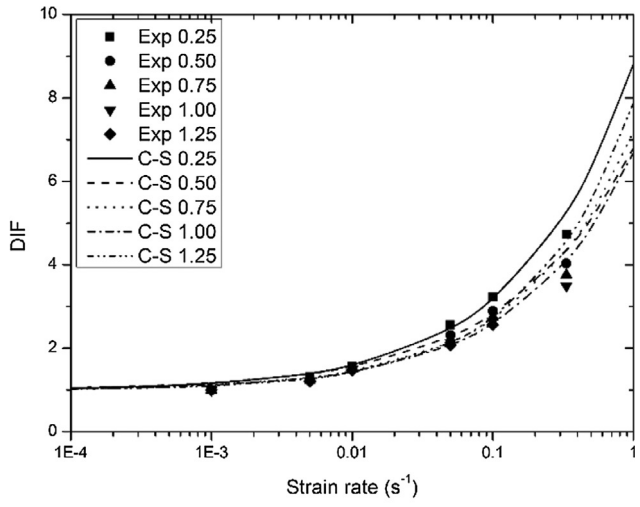

(a)

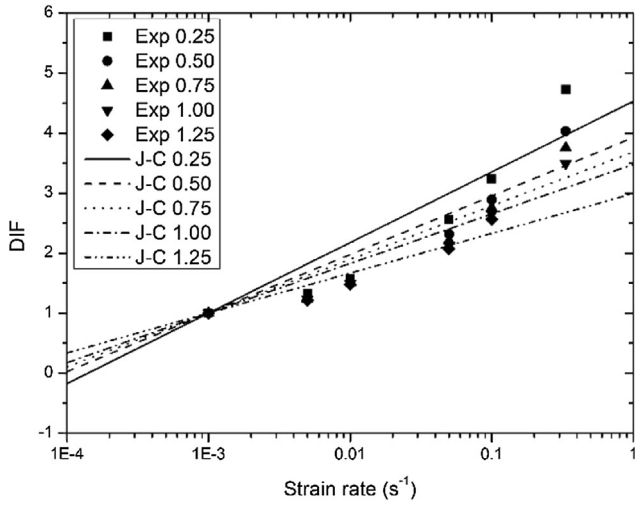

(b)

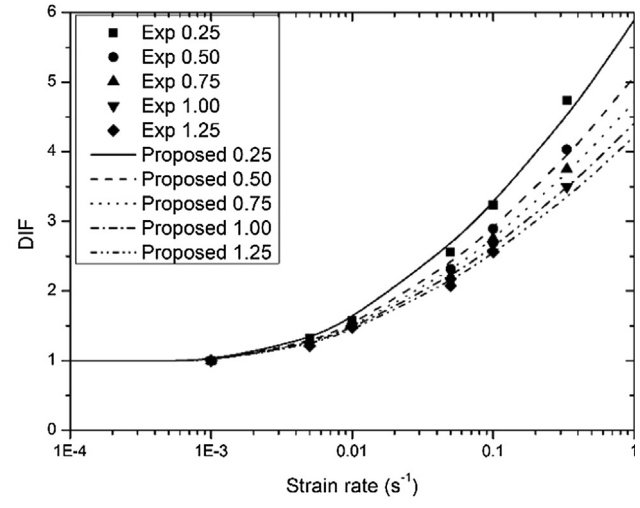

(c)

Fig. 6. Comparison of different viscoplastic and viscoelastic models with the cumulative strain energy enhancement under different strain levels, (a) Cowper-Symonds; (b) Johnson-Cook; and (c) proposed models.

2.3.1. Modified viscoelastic Mooney-Rivlin models

The modified rate-dependent Cowper–Symonds Mooney–Rivlin strain energy potential is given in Eq. (20), and the Cauchy (true) stress models are presented in Eq. (21).

$$W = \psi(\bar{I}_1, \bar{I}_2)\left(1 + \left(\frac{\dot{\varepsilon}}{D}\right)^{\frac{1}{q}}\right) \tag{20}$$

$$\sigma = 2(\lambda^2 - \frac{1}{\lambda})(\frac{\partial \psi}{\partial \bar{I}_1} + \frac{1}{\lambda}\frac{\partial \psi}{\partial \bar{I}_2})\left(1 + \left(\frac{\dot{\varepsilon}}{D}\right)^{\frac{1}{q}}\right) \tag{21}$$

The modified rate-dependent Johnson–Cook Mooney–Rivlin strain energy potential is provided in Eq. (22), and the Cauchy (true) stress models is presented in Eq. (23). These two models were studied by Mohotti et al. [23] comparison was undertaken with the other proposed models in this study.

$$W = \psi(\bar{I}_1, \bar{I}_2)\ (1 + C\ln\dot{\varepsilon}^*) \tag{22}$$

$$\sigma = 2(\lambda^2 - \frac{1}{\lambda})(\frac{\partial \psi}{\partial \bar{I}_1} + \frac{1}{\lambda}\frac{\partial \psi}{\partial \bar{I}_2})\ (1 + C\ln\dot{\varepsilon}^*) \tag{23}$$

The proposed rate-dependent Mooney–Rivlin strain energy potential is indicated in Eq. (24), and the Cauchy (true) stress model is given in Eq. (25).

$$W = \psi(\bar{I}_1, \bar{I}_2)\left(1 + \frac{1}{A}(\ln\dot{\varepsilon}^*)^B\right) \tag{24}$$

$$\sigma = 2(\lambda^2 - \frac{1}{\lambda})(\frac{\partial \psi}{\partial \bar{I}_1} + \frac{1}{\lambda}\frac{\partial \psi}{\partial \bar{I}_2})\left(1 + \frac{1}{A}(\ln\dot{\varepsilon}^*)^B\right) \tag{25}$$

2.3.2. Modified viscoelastic Ogden models

The modified rate-dependent Cowper–Symonds Ogden strain energy potential is given in Eq. (26), and the Cauchy (true) stress model is presented in Eq. (27).

$$W = \sum_{i=1}^{N} \frac{\mu_i}{\alpha_i}(\lambda^{\alpha_i} + \frac{2}{\lambda^{\alpha_i/2}} - 3)\left(1 + \left(\frac{\dot{\varepsilon}}{D}\right)^{\frac{1}{q}}\right) \tag{26}$$

$$\sigma = \frac{\partial W}{\partial \lambda} = \sum_{i=1}^{N} \mu_i(\lambda^{\alpha_i - 1} + \frac{2}{\lambda^{\frac{\alpha_i}{2}+1}} - 3)\left(1 + \left(\frac{\dot{\varepsilon}}{D}\right)^{\frac{1}{q}}\right) \tag{27}$$

The modified rate-dependent Johnson–Cook Ogden strain energy potential is provided in Eq. (28), and the Cauchy (true) stress model is presented in Eq. (29).

$$W = \sum_{i=1}^{N} \frac{\mu_i}{\alpha_i}(\lambda^{\alpha_i} + \frac{2}{\lambda^{\alpha_i/2}} - 3)\ (1 + C\ln\dot{\varepsilon}^*) \tag{28}$$

$$\sigma = \frac{\partial W}{\partial \lambda} = \sum_{i=1}^{N} \mu_i(\lambda^{\alpha_i - 1} + \frac{2}{\lambda^{\frac{\alpha_i}{2}+1}} - 3)\ (1 + C\ln\dot{\varepsilon}^*) \tag{29}$$

Table 4
The material model parameter of each viscoplastic and viscoelastic models for the cumulative strain energy enhancement.

Cowper-Symonds model		Johnson-Cook model	Proposed model	
D	q	C	A	B
0.0398	1.6072	0.3932	11.2391	1.9779

The proposed rate-dependent Ogden strain energy potential is indicated in Eq. (30), and the Cauchy (true) stress model is given in Eq. (31).

$$W = \sum_{i=1}^{N} \frac{\mu_i}{\alpha_i}(\lambda^{\alpha_i} + \frac{2}{\lambda^{\alpha_i/2}} - 3)\left(1 + \frac{1}{A}(\ln\dot{\varepsilon}^*)^B\right) \quad (30)$$

$$\sigma = \frac{\partial W}{\partial \lambda} = \sum_{i=1}^{N} \mu_i(\lambda^{\alpha_i - 1} + \frac{2}{\lambda^{\frac{\alpha_i}{2}+1}} - 3)\left(1 + \frac{1}{A}(\ln\dot{\varepsilon}^*)^B\right) \quad (31)$$

3. Experimental program

3.1. Materials

Palm-based polyol (PKO-p) [51,52] was supplied by the Polymer Research Center (PORCE) of the Universiti Kebangsaan Malaysia (Bangi, Malaysia). 4,4-Diphenylmethane diisocyanate (MDI) was obtained from Cosmopolyurethane Sdn. Bhd., Kuala Lumpur, Malaysia. Acetone (industrial grade) and polyethylene glycol (PEG: Mw 200 Da) were purchased from Sigma Aldrich (M) Sdn. Bhd., Malaysia, Petaling Jaya, Malaysia.

3.2. Preparations of the PU elastomers

A PU resin was prepared using the solution-casting technique from the rapid reaction between PKO-p and MDI via the pre-polymerization technique in the presence of PEG as the plasticizer. The ratio of PKO-p: MDI: PEG was 100:80:6, and PU resin was prepared as pre-cast sheets with a thickness of approximately 3 mm. A clear yellowish and bubble-free PU sheet was obtained and left under the condition of ambient temperature for further characterization.

3.3. Tensile test

The tensile mechanical behavior of the PU at varying strain rates was examined using an Instron model 5566 testing machine (Instron Corporation, Canton, MA, USA) under the displacement-controlled method (constant engineering strain rate). Dumbbell test specimens were chopped from the cured pre-cast PU sheets using Die C, as specified in ASTM D 412: Method-A [Fig. 2(a)]. Each specimen was chopped in the same direction in the PU sheet to minimize the effect of anisotropy or grain directionality caused by the flow direction during preparation and processing. The specimen dimensions were measured using a vernier caliper with an accuracy of 0.01 mm, and the average of three measurements was used for each dimension (width and thickness). Griping was conducted automatically to avoid the influence of clamping pressure because elastomeric materials are extremely sensitive to clamping pressure. The uniaxial tensile tests were conducted at varying strain rates between 0.001 s^{-1} and 0.33 s^{-1} by achieving different crosshead speeds [Fig. 2(b)] (the maximum grip velocity of the machine used was 500 mm/min, which corresponded to the strain rate of 0.33 s^{-1} for the test specimens used). All tests were performed at an ambient temperature of approximately 22 °C. The entire test was controlled through a computer with highly rated software (Blue Hill v2.5, Instron Corporation, Canton, MA, USA). Data acquisition (time, load, and deflection) was conducted using the same software until the failure of specimens. For each strain level, a minimum six samples were tested. Average curve was used to simulate the behavior at each strain level as shown in Fig. 3.

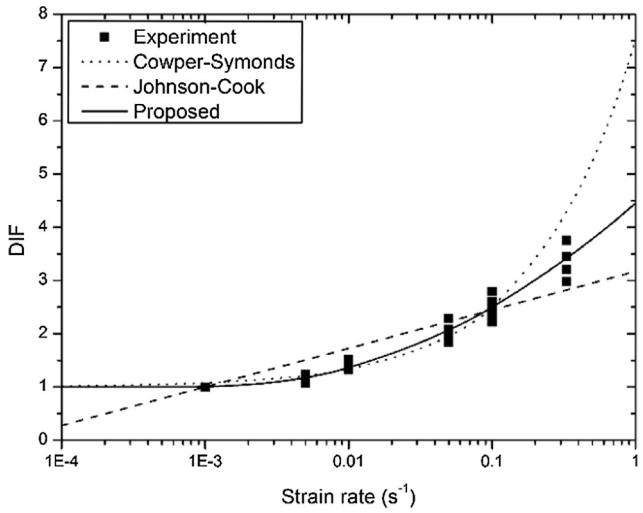

Fig. 7. Comparison of different viscoplastic and viscoelastic models with the cumulative strain energy enhancement.

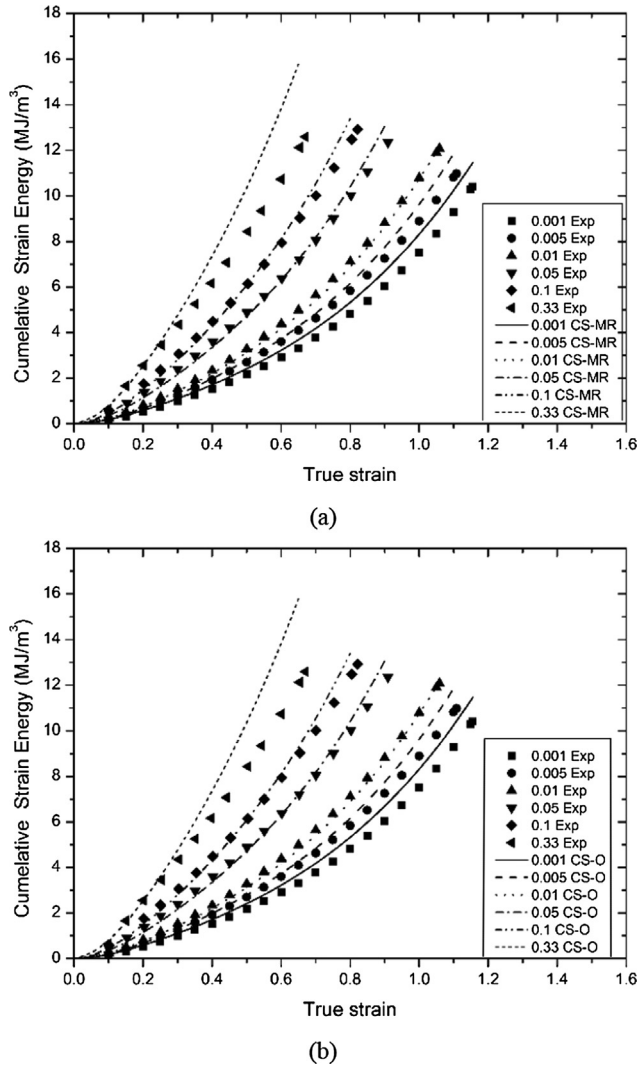

Fig. 8. Comparison of modified Cowper-Symonds hyperelastic models with experimental data to predict the cumulative strain energy of the PU sample (a) Nine-parameter Mooney-Rivlin; and (b) Three-parameter Ogden models.

4. Experimental results

The extensive use of PUs in the modern design industry as a strengthening, retrofitting, protective, and composite material highlights the necessity of observing its material properties, particularly their tensile mechanical characteristics, such as Young's modulus, yield, ultimate and failure stresses, and failure strain. Accordingly, a discussion on these properties obtained from a series of experimental studies and their rate dependency is documented in the following section. The universal testing machine has been extensively used to investigate the tensile characteristics of elastomeric materials. The mechanics of the strain rate-dependent behavior of the PU sample was elucidated in experiments, in which homogeneous dynamic deformation processes (constant engineering strain rates) were achieved over the tested strain rate regimes. Fig. 3(a) plots the engineering stress–strain curves of the PU sample investigated in this study at various strain rates and their comparison. The actual strain rate in each specimen was calculated by differentiating strain–time history and showed a uniform strain rate condition throughout the test duration under each strain rate level. Stress–strain non-linearity and high rate dependence were observed under each stress strain level. For all the specimens, a single break point at arbitrary locations was observed during the failure, and only the specimens that failed within their gauge length were used for further analysis.

The initial elastic region showed the typical behavior of an elastic–plastic material over tested strain rate regimes. After the linear stress–strain region with substantial stress and elongation, PU started yielding, as shown in Fig. 3(a), under all strain rate conditions. The further increase in the loads above the elastic limit initiated the breakdown of the two-phase structure (soft and hard segments) because of the breakdown of cross-linkages. This phenomenon caused the sliding of hard segments relative to their neighboring segments within the hard domains, fragmenting the original hard domains into several smaller units, stripping of segments from the hard domains, and the formation of a new soft matrix within the hard domains. Irreversible deformations and residual strain then occurred in the material. The PU reached its ultimate tensile stress before its failure caused by the strain hardening mechanism under all tested strain rate levels. However, a decrement in the strain hardening behavior was shown with increasing strain rate, thereby resulting in decreased tangent modulus. Similarly, failure strain was inversely correlated with

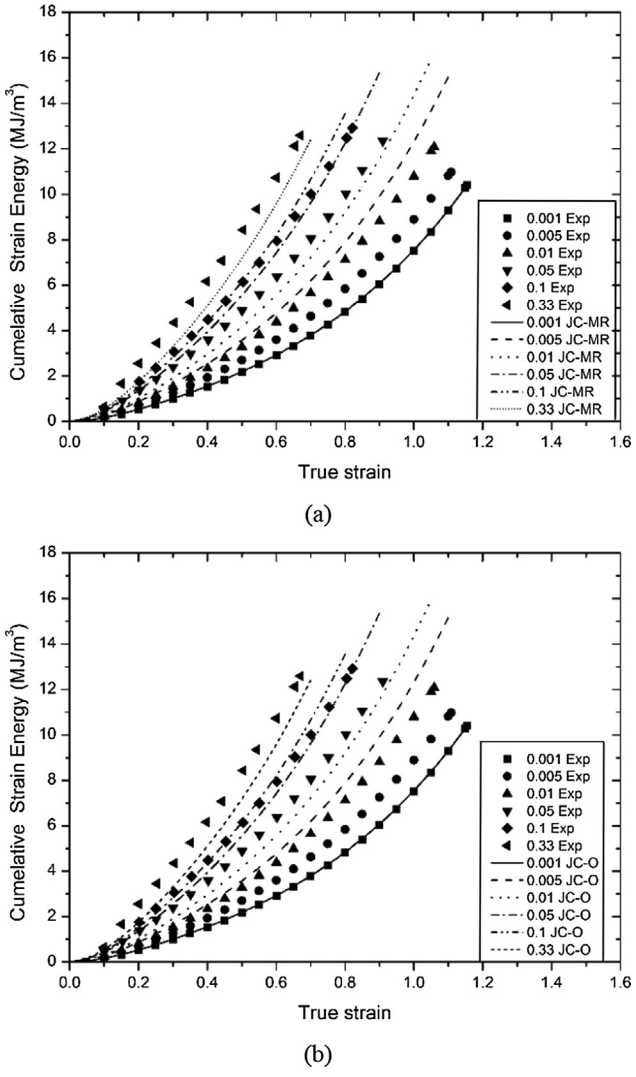

Fig. 9. Comparison of modified Johnson-Cook hyperelastic models with experimental data to predict the cumulative strain energy of the PU sample (a) Nine-parameter Mooney-Rivlin; and (b) Three-parameter Ogden models.

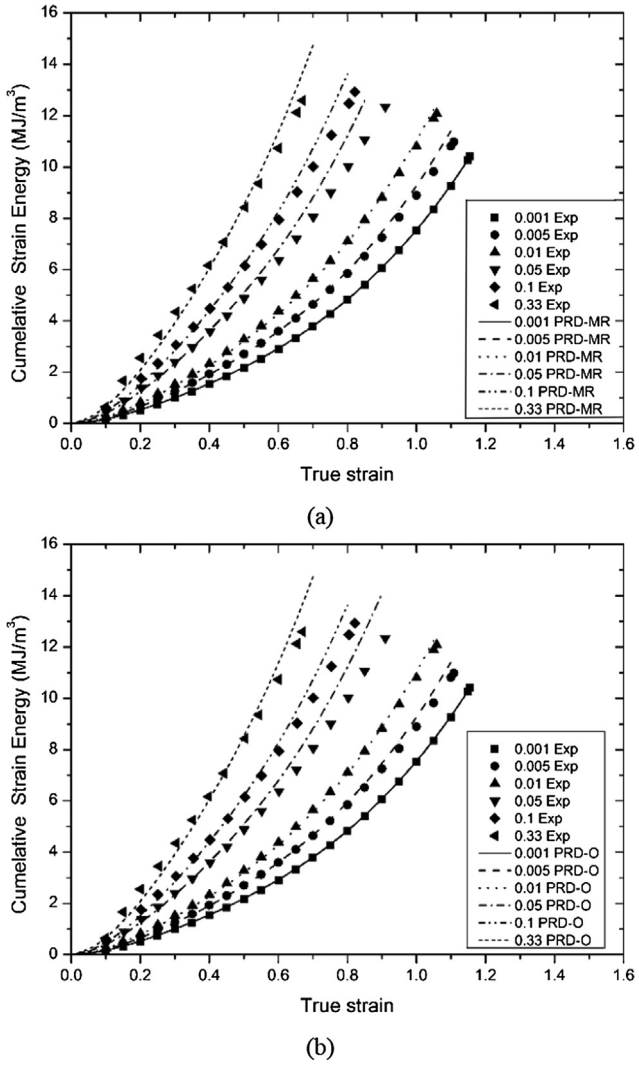

Fig. 10. Comparison of modified hyperelastic models with experimental data to predict the cumulative strain energy of the PU sample (a) Nine-parameter Mooney-Rivlin; and (b) Three-parameter Ogden models.

strain rate. Comprehensively, the enhancement in Young's modulus and all stresses were exhibited with increasing strain rates by analyzing the change in stress–strain profiles. A dramatic transition from "rubbery" to "leathery" features of elastomeric PU was observed with strain rate.

Strain energy density was computed by integrating the area underneath the stress–strain curve. As shown in Fig. 3(b), the strain energy density increased with increasing strain rates. Consequently, the material absorbed a high quantity of energy before its failure under high strain rate conditions. In particular, enhancement in the cumulative strain energy was shown under both resilience and toughness modulus characteristics. This finding signified the importance of studying the influence of strain rate on strain energy density, which was the pre-requirement for modeling constitutive equations in this study. Considering the inclusive behavior, the PU could be defined as a material that is hyper-viscoelastic. A detailed discussion on the experimental study is documented in a subsequent publication by the authors. The tensile mechanical properties of the tested PU are provided in Table 2.

5. Material models

5.1. Tensile characteristics

The DIF of each mechanical tensile property of the PU under different strain levels was calculated by taking the ratio between the particular property and the material property at reference strain rate level, which was 0.001 s^{-1} in this study. From the results presented in Table 1, the DIF values for the main tensile properties were plotted against strain rates, as shown in Fig. 4(a–h). From the analysis, the correlation between DIF and strain rates was established using the three viscoplastic and viscoelastic models discussed, namely, Cowper–Symonds, Johnson–Cook, and the proposed model. As shown in Fig. 4(a, b, d, e, g, and h), clear increases in Young's modulus, yield stress, ultimate tensile stress, failure stress, resilience modulus, and toughness modulus were observed with increasing strain rate. This behavior evidently emphasized a significant enhancement in tensile mechanical properties with increasing strain rates. Accordingly, strain rate-dependent material constitutive models are necessary to characterize the behavior of elastomeric materials under varying strain rates. The existing

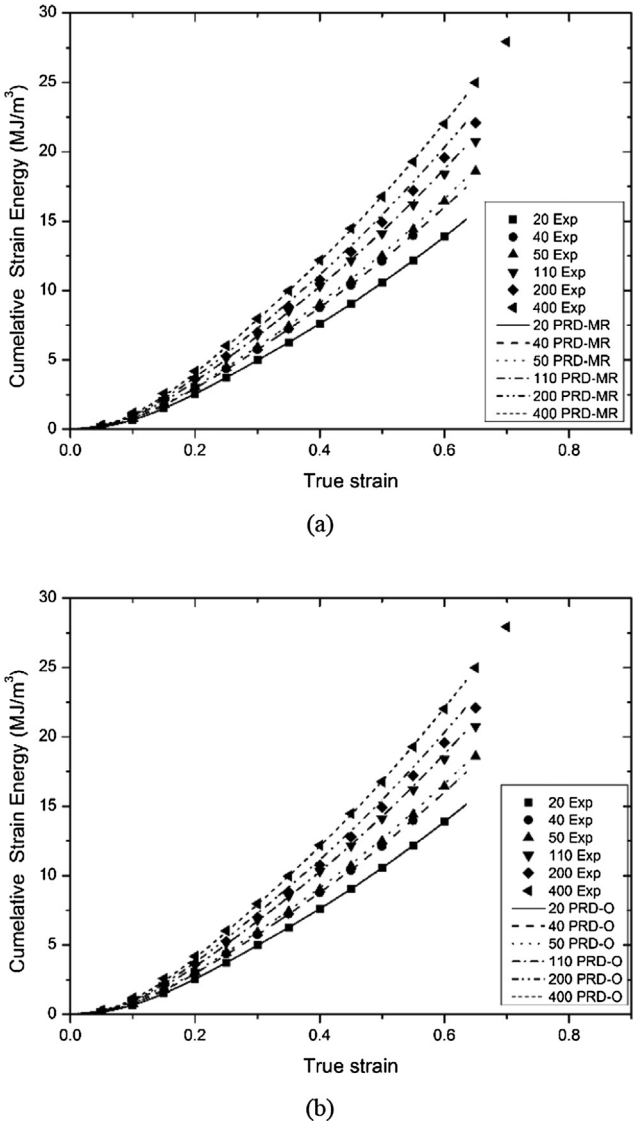

Fig. 11. Comparison of modified hyperelastic models with experimental data to predict the cumulative strain energy with experimental data reported by Mohotti et al. [23] (a) Nine-parameter Mooney-Rivlin; and (b) Three-parameter Ogden models.

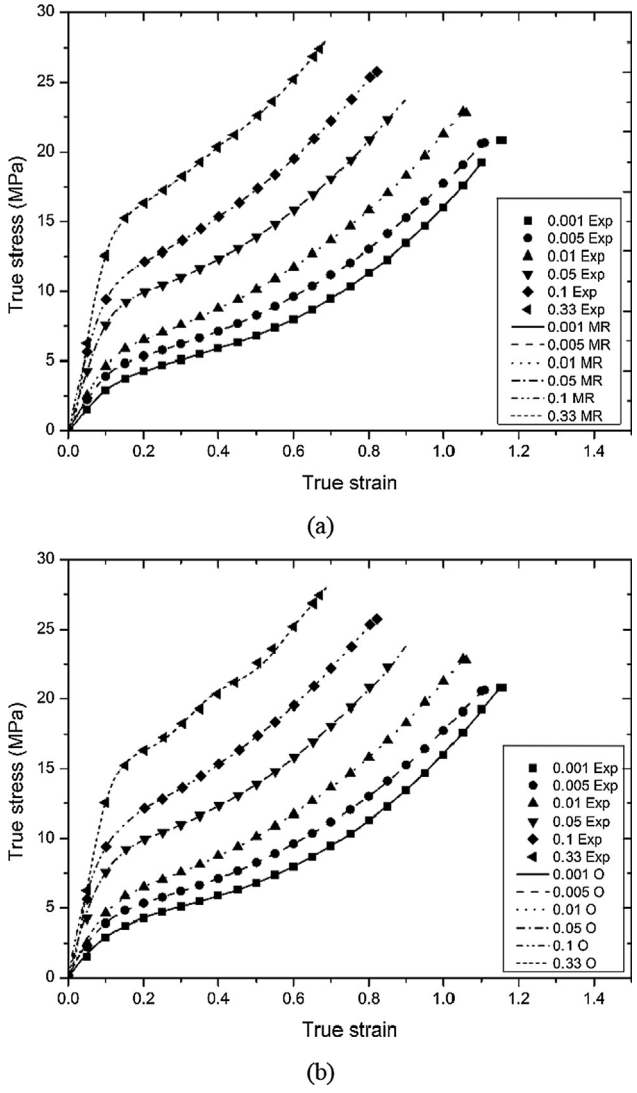

Fig. 12. Comparison of original hyperelastic model with experimental data to predict the stress–strain behaviour of the PU sample (a) Nine-parameter Mooney-Rivlin; and (b) Three-parameter Ogden models.

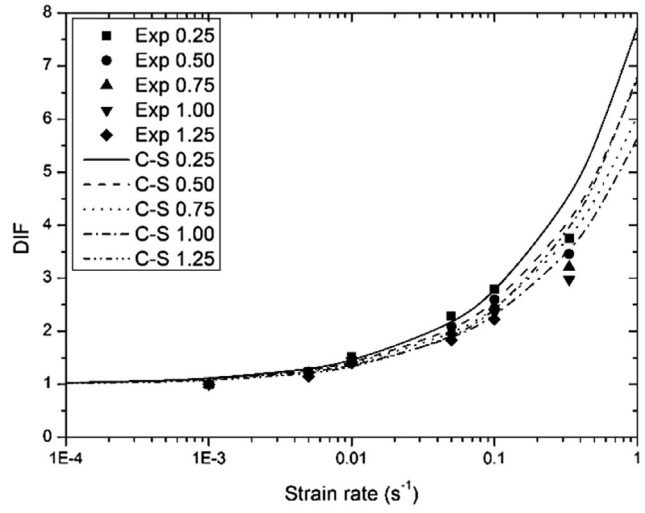

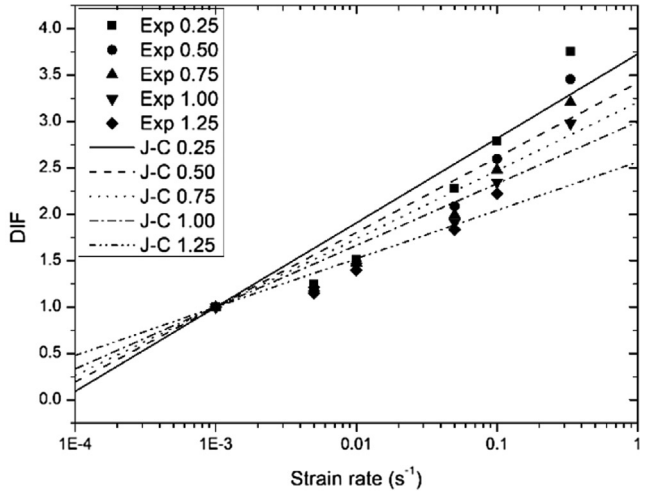

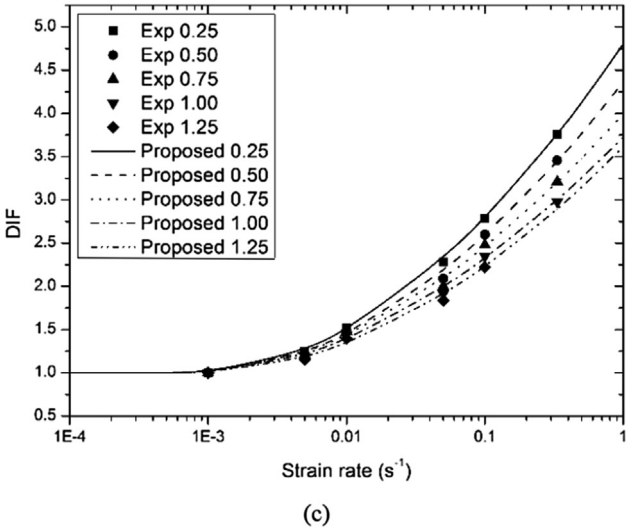

Fig. 13. Comparison of different viscoplastic and viscoelastic models with the true stress enhancement under different strain levels, (a) Cowper-Symonds; (b) Johnson-Cook; and (c) proposed models.

hyper-elastic models that incorporate strain rate effects should also be modified. However, tangent modulus and failure strain decreased, as shown in Fig. 4(c) and (f). The effect of the decrement

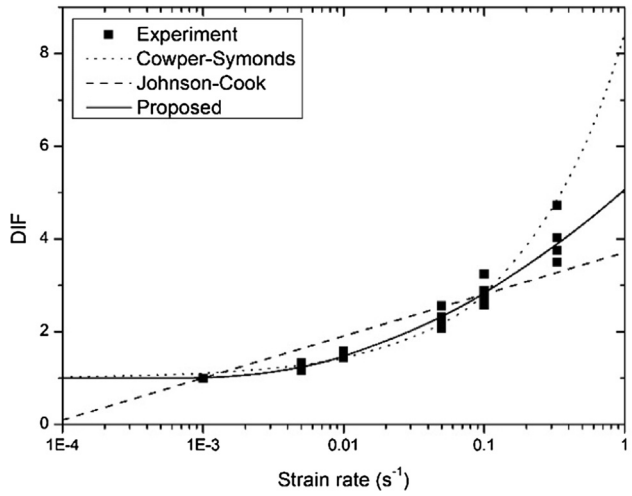

Fig. 14. Comparison of different viscoplastic and viscoelastic models with the true stress enhancement.

in these properties on the rate-dependent material models is discussed in the subsequent section.

The coefficients of each viscoelastic models for the DIF of each tensile material property, as obtained based on the experimental findings, are provided in Table 2. The variation in the tangent modulus and failure strain was represented using the modified Cowper–Symonds, the modified proposed models, and the original Johnson–Cook model. The coefficient of determination, R^2, obtained for each tensile property from the linear correlation of each viscoplastic and viscoelastic model is indicated in Table 3. As shown in Fig. 4(a)–(h) and in Table 3, the proposed viscoelastic model exhibited the best representation of the DIF–strain rate relationship for all tensile characteristics, except tangent modulus. All the three models were further used to evaluate the accuracy of hyper-viscoelastic models, as stated in Section 2.2.

5.2. Cumulative strain energy models

The main focus was on the strain energy absorption capacity throughout the tensile deformation process in this study. As observed in the previous section, the strain energy density of the tested PU exhibited rate dependency during the elastic, plastic limit, and failure processes. This behavior was shown in the results presented in Fig. 4(g) and (h), which depict a clear enhancement in the energy absorption capacity with DIFs of 3.35 and 1.31 for resilience modulus and toughness modulus, respectively, from the strain rate of 0.001–0.33 s^{-1}. This result emphasized the requirement for materials that are suitable for dynamic applications that absorb more energy under high strain rate conditions than under low strain rate conditions. This behavior also contributed positively to the application of protective coatings for high-impulsive applications by reducing material consumption. Therefore, the use of hyper-viscoelastic material models is important to predict material behavior under varying strain rate conditions.

Table 5
The material model parameter of each viscoplastic and viscoelastic models for the true stress enhancement.

Cowper-Symonds model		Johnson-Cook model	Proposed model	
D	q	C	A	B
0.0554	1.5421	0.3141	15.88698	2.0722

The material constants of the nine-parameter Mooney–Rivlin and the three-parameter Ogden models were determined using the experimental data under each strain rate via the curve-fitting method. As shown in Fig. 5, the accuracy of the fitted parameters was checked by plotting the cumulative energy versus strain graphs for each strain rate level tested and compared with the experimental results. Fig. 5 shows that the curve-fitting results of both the Mooney–Rivlin and Ogden models are in good agreement with the experimental data. This finding confirmed the suitability of these models to represent the non-linear behavior of elastomeric materials. However, the original Mooney–Rivlin and Ogden models were rate-insensitive and could not predict the strain rate effect accurately. During dynamic loading conditions, materials undergo different strain rate conditions and strain rate changes with time. Therefore, an analysis with a rate-insensitive constitutive model, which the material behavior defined at a certain strain rate level, can provide inaccurate outcomes.

The hyper-elastic term of the hyper-viscoelastic material models could be derived by investigating simple tension or compression behavior at a predefined strain rate. This predefined strain rate would be considered the reference strain rate in the hyper-viscoelastic material models. 0.001 s^{-1} was regarded as the reference strain rate in this study. Fig. 6 plots the cumulative strain energy enhancement with the three viscoplastic and viscoelastic models for five different strain levels independently under varying strain rates. The cumulative strain energy enhancement under different strain levels was nearly equal and could be defined with one viscoplastic or viscoelastic model for all strain levels. Thus, the strain energy enhancement was defined by one constitutive equation for each viscoplastic and viscoelastic model. The models are plotted in Fig. 7. The material model parameter of each viscoplastic and viscoelastic model for DIF was derived by considering the reference strain rate as 0.001 s^{-1}, as provided in Table 4. The coefficients of determination, R^2, obtained for each viscoplastic and viscoelastic model from the linear correlation were 0.9542, 0.8216, and 0.9748 for the Cowper–Symonds, Johnson–Cook, and proposed viscoelastic models, respectively. As shown in Fig. 7 and from the coefficients of determination, the proposed viscoelastic model showed the best representation of the DIF–strain rate relationship of cumulative strain energy.

The obtained hyper-elastic material models were also used to predict the material behavior at other strain rates, which were used in the experimental analysis and compared with the experimental results, as presented in Figs. 8–10. The hyper-viscoelastic models

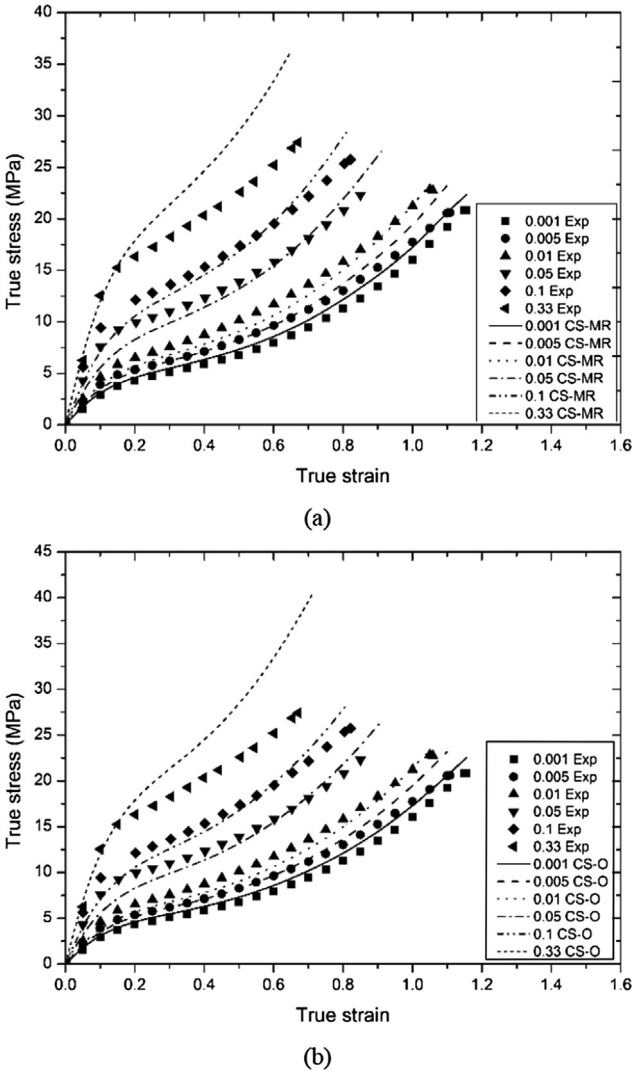

Fig. 15. Comparison of modified Cowper-Symonds hyperelastic models with experimental data to predict the true stress of the PU sample (a) Nine-parameter Mooney-Rivlin; and (b) Three-parameter Ogden models.

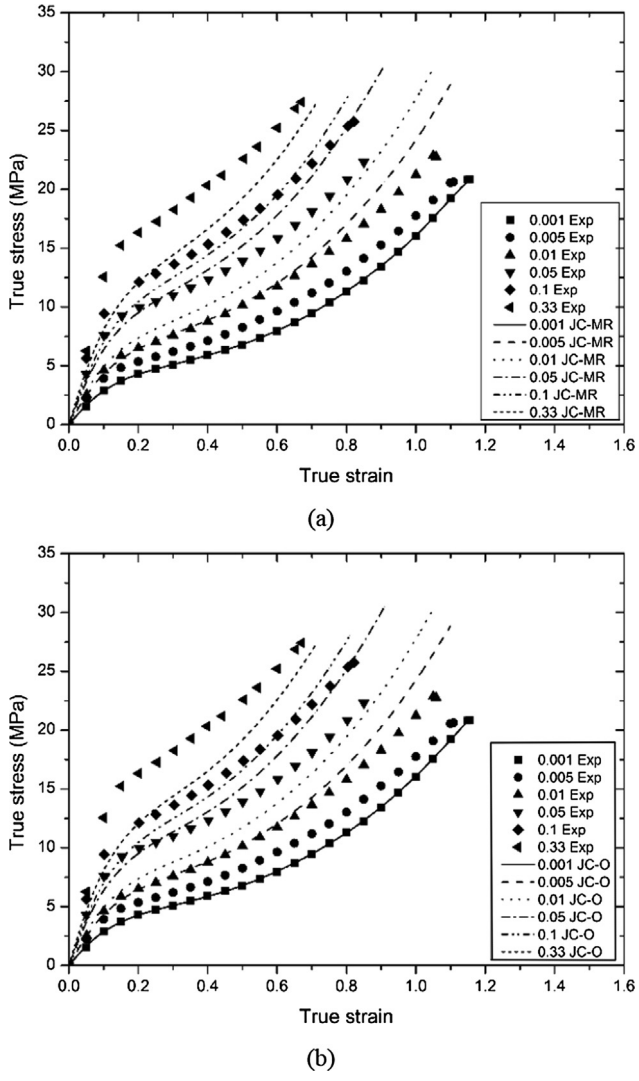

Fig. 16. Comparison of modified Johnson-Cook hyperelastic models with experimental data to predict the true stress of the PU sample (a) Nine-parameter Mooney-Rivlin; and (b) Three-parameter Ogden models.

formed with the proposed viscoelastic model agree with the experimental results over the strain rate regime considered in this study. The hyper-viscoelastic models formed with the Cowper–Symonds showed slight over estimation at higher strain rate levels, and subsequently the hyper-viscoelastic models formed with Johnson–Cook model showed under estimation at higher strain rate level. The hyper-viscoelastic models formed with the proposed viscoelastic model exhibited best capability of predicting material behavior with the strain rate effect of elastomeric PU or similar materials. In addition, these models would be suitable to modify the rate-insensitive material models encoded in the FE model (FEM) codes by incorporating the strain rate parameter into the existing codes. In addition, the hyper-viscoelastic strain energy models formed with the proposed viscoelastic model were further verified with the experimental results reported by Mohotti et al. [23] on elastomeric polyurea, as given in Fig. 11. The proposed model prediction shows good agreement with the experimental data.

5.3. Stress–strain models

All stresses showed rate dependency throughout the entire deformation, as reported earlier. Figs. 3(a) and 4(b, d, and e) provide evidence for this behavior, which depict clear enhancements in the stresses with DIFs of 3.88, 2.08, and 2.25 for yield stress, ultimate tensile stress, and failure stress, respectively, from the strain rates of 0.001–0.33 s^{-1}. The material stiffened under higher strain-rate condition and failed at high stresses, which were an ideal characteristic for applying protective coatings for highly impulsive applications. As shown in Fig. 12, the parameters obtained in the previous section were used to plot the true stress versus true strain graphs for different strain rate levels tested and compared with the experimental results. Fig. 12 shows that the curve-fitting results of both the Mooney–Rivlin and Ogden models are in good agreement with the experimental data. Fig. 13 plots the tensile stress enhancement with the each viscoplastic and viscoelastic models for five different strain levels independently under varying strain rates. The stress enhancement under different strain levels was nearly equal and could be defined with one viscoplastic or viscoelastic model for all strain levels similar to the cumulative strain energy. Hence, the stress enhancement was defined using one constitutive equation for each viscoplastic and viscoelastic model. The models are plotted in Fig. 14. The material model parameter of each viscoplastic and viscoelastic model for DIF was derived, as provided in Table 5. The coefficients of determination, R^2, obtained for each viscoplastic

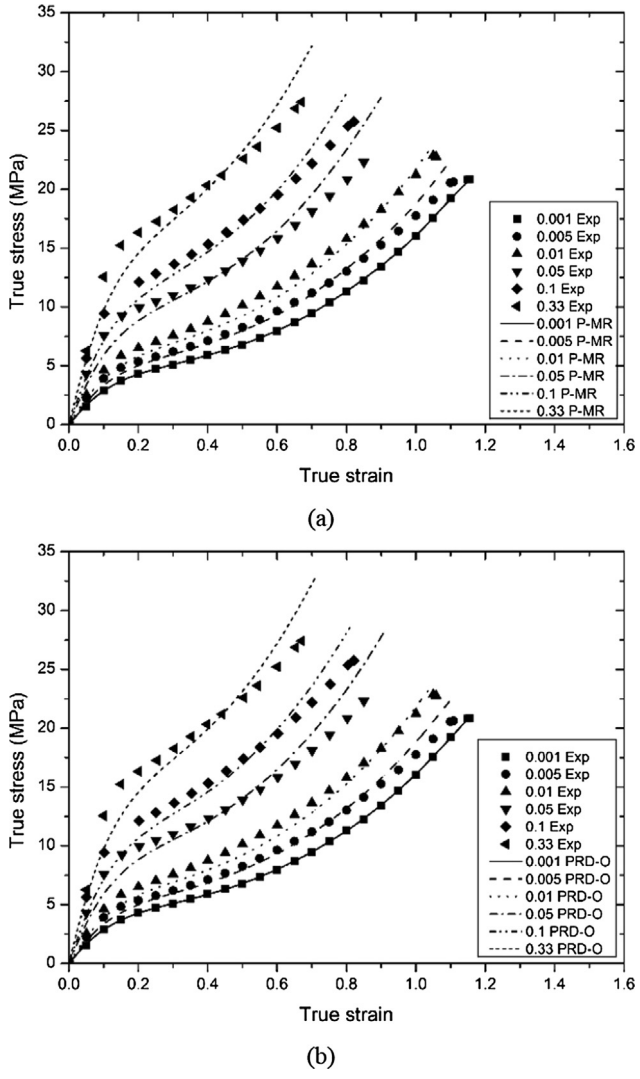

Fig. 17. Comparison of modified hyperelastic models with experimental data to predict the true stress of the PU sample (a) Nine-parameter Mooney-Rivlin; and (b) Three-parameter Ogden models.

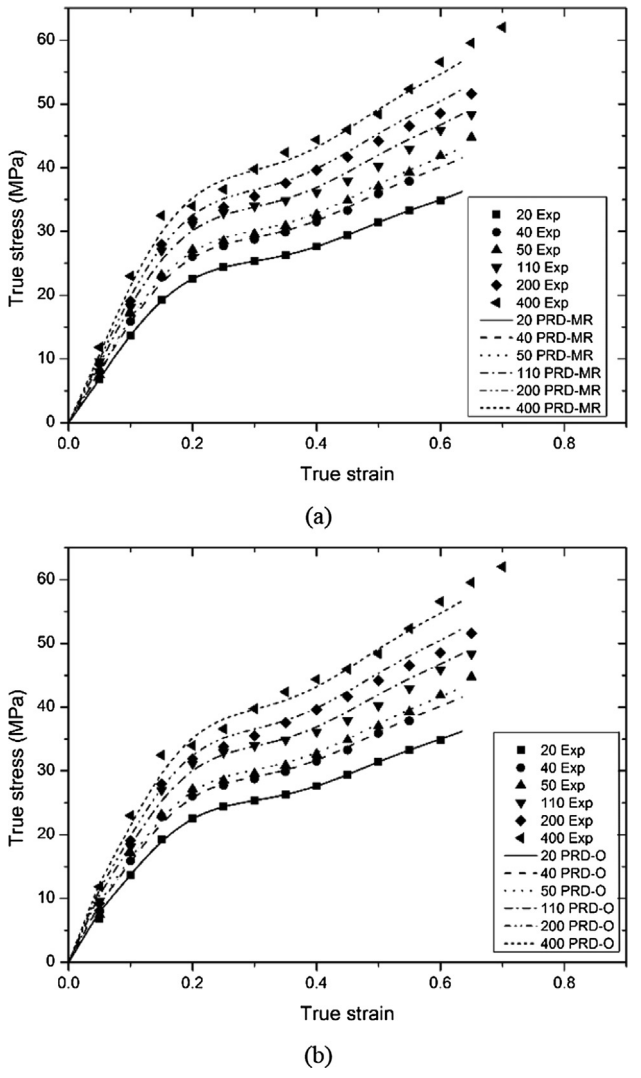

Fig. 18. Comparison of modified hyperelastic models with experimental data to predict the true stress with experimental data reported by Mohotti et al. [23] (a) Nine-parameter Mooney-Rivlin; and (b) Three-parameter Ogden models.

and viscoelastic model from the linear correlation were 0.9496, 0.7875, and 0.9653 for the Cowper–Symonds, Johnson–Cook, and proposed viscoelastic models, respectively. Fig. 14 and the coefficients of determination validated that the proposed viscoelastic model was the best representation of the DIF–strain rate relationship of true stress.

In Figs. 15–17, analytical curves are plotted using the obtained hyper-viscoelastic material models at other strain rates and compared with the experimental results. Similar to that observed in the cumulative strain energy models, the hyper-viscoelastic stress–strain models formed with the Cowper–Symonds model showed slight over estimation at higher strain rate levels. The hyper-viscoelastic stress–strain models formed with Johnson–Cook model showed under estimation at higher strain rate level and over estimation at lower strain rate level. The hyper-viscoelastic stress–strain models formed with the proposed viscoelastic model showed the best prediction with the experimental results over the strain rate regime considered in this study. The hyper-viscoelastic stress–strain models formed with the proposed viscoelastic model were further verified with the experimental results reported by Mohotti et al. [23] on elastomeric polyurea, as given in Fig. 18. The proposed model prediction shows good agreement with the experimental data.

6. Conclusions

A novel viscoelastic and hyper-viscoelastic constitutive models were developed and validate in this study using the experimental findings of the dynamic tensile properties of a PU sample under varying strain rates (0.001–0.33 s^{-1}). The stress–strain behavior of the PU sample over the tested strain regimes was considerably non-linear, and were highly rate dependent. A dramatic transition in its mechanical behavior was exhibited, from rubbery to leathery behavior, with increasing strain rates. One of the crucial findings of this study was that the proposed viscoelastic model showed the best correlation to represent the enhancement of the mechanical properties under varying strain rate conditions compared with the Cowper–Symonds and Johnson–Cook models. The original Mooney–Rivlin and Ogden models accurately presented the behavior of the PU material at varying strain rates with different sets of model parameters that were derived individually for each strain rate. The proposed hyper-viscoelastic models by incorporating the viscoelastic models mentioned above into those hyper-elastic models were used to predict the rate-dependent non-linear behavior of the PU sample. These proposed hyper-viscoelastic models could be used to predict the material behavior using only one set of hyper-elastic model parameters at a certain strain rate, in combination with the viscoelastic model parameters. The hyper-viscoelastic cumulative strain energy and stress–strain models developed with the proposed viscoelastic model showed high capability of predicting the material behavior with the strain rate effect of elastomeric PU or similar materials. These models would be suitable to modify the rate-insensitive material models encoded in FEM codes by incorporating the strain rate parameter into the existing codes. Furthermore, the hyper-viscoelastic strain energy models developed with the proposed viscoelastic model were verified with the experimental results on elastomeric polyurea reported in the literature and showed good agreement with the experimental data.

Author contributions

The experimental and analytical work were designed and performed by H.M.C.C. Somarathna under the guidance and supervision of S.N. Raman, A.A. Mutalib, and K.H. Badri. The data processing and analysis, model formulation, and analytical investigations were performed by H.M.C.C. Somarathna, S.N. Raman, and D. Mohotti, with the assistance from A.A. Mutalib and K.H. Badri. The manuscript was written together by H.M.C.C. Somarathna, S. N. Raman and D. Mohotti, and was supplemented by the contributions from A.A. Mutalib, and K.H. Badri.

Declaration of Competing Interest

The authors declare that they have no known competing financial interests or personal relationships that could have appeared to influence the work reported in this paper.

Acknowledgement

The authors would like to extend their gratitude to Universiti Kebangsaan Malaysia and the Ministry of Education, Malaysia for providing the necessary funding for this research through the Impak Perdana Grant (DIP-2017-002), and to the Polymer Research Centre of UKM for the generous supply of palm-based polyol.

References

[1] H.M.C.C. Somarathna, S.N. Raman, D. Mohotti, A.A. Mutalib, K.H. Badri, The use of polyurethane for structural and infrastructural engineering applications: A state-of-the-art review, Constr. Build. Mater. 190 (2018) 995–1014, https://doi.org/10.1016/j.conbuildmat.2018.09.166.
[2] H.M.C.C. Somarathna, S.N.N. Raman, A.A.A. Mutalib, K.H.H. Badri, Elastomeric polymers for blast and ballistic retrofitting of structures, J. Teknol. 76 (2015), https://doi.org/10.11113/jt.v76.3608.
[3] S.N. Raman, Polymeric Coatings for Enhanced Protection of Reinforced Concrete Structures from the Effects of Blast, The University of Melbourne, Australia, 2011.
[4] S.N. Raman, T. Ngo, P. Mendis, T. Pham, Elastomeric polymers for retrofitting of reinforced concrete structures against the explosive effects of blast, Adv. Mater. Sci. Eng. 2012 (2012) 1–8, https://doi.org/10.1155/2012/754142.
[5] H.M.C.C. Somarathna, S.N. Raman, A.A. Mutalib, K.H. Badri, Mechanical characterization of polyurethane elastomers: for retrofitting application against blast effects, in: Proceedings Third Conf. Smart Monit. Assess. Rehabil. Struct. (SMAR 2015), Antalya, Turkey, 2015, pp. 82–89. https://scholar.google.com/citations?user=D0UxtzwAAAAJ&hl=en#d=gs_md_cita-d&p=&u=%2Fcitations%3Fview_op%3Dview_citation%26hl%3Den%26user%3DD0UxtzwAAAAJ%26citation_for_view%3DD0UxtzwAAAAJ%3A9yKSN-GCB0IC%26tzom%3D-330.
[6] H.M.C.C. Somarathna, S.N. Raman, K.H. Badri, A.A. Mutalib, D. Mohotti, S. Engineering, S.D. Ravana, Quasi-static behavior of palm-based elastomeric polyurethane: for strengthening application of Structures under impulsive loadings, Polymers (Basel) (2016), https://doi.org/10.3390/polym8050202.
[7] L. Dai, C. Wu, F. An, S. Liao, Experimental investigation of polyurea-coated steel plates at underwater explosive loading, Adv. Mater. Sci. Eng. 2018 (2018) 1–7, https://doi.org/10.1155/2018/1264276.
[8] A.A. Kruglikov, V.A. Yavna, Y.M. Ermolov, A.G. Kochur, Z.B. Khakiev, Strengthening of the railway ballast section shoulder with two-component polymeric binders, Transp. Geotech. 11 (2017) 133–143, https://doi.org/10.1016/J.TRGEO.2017.05.004.
[9] K.J. Knox, M.I. Hammons, T.T. Lewis, J.R. Porter, Polymer Materials for Structural Retrofit, Tyndall AFB: Panama City, FL, USA, 2000.
[10] J.S. Davidson, J.W. Fisher, M.I. Hammons, J.R. Porter, R.J. Dinan, Failure Mechanisms of Polymer-Reinforced Concrete Masonry Walls Subjected to Blast, 2005.
[11] T.D. Hrynyk, J.J. Myers, F. Asce, Out-of-Plane Behavior of URM Arching Walls with Modern Blast Retrofits : Experimental Results and Analytical Model, 2008, pp. 1589–1597.
[12] K. Ackland, C. Anderson, T.D. Ngo, T. Duc, Deformation of polyurea-coated steel plates under localised blast loading, Int. J. Impact Eng. 51 (2013) 13–22, https://doi.org/10.1016/J.IJIMPENG.2012.08.005.
[13] D. Mohotti, T. Ngo, S.N. Raman, M. Ali, P. Mendis, Plastic deformation of polyurea coated composite aluminium plates subjected to low velocity impact, Mater. Des. 56 (2014) 696–713, https://doi.org/10.1016/j.matdes.2013.11.063.
[14] D. Mohotti, T. Ngo, P. Mendis, S.N. Raman, Polyurea coated composite aluminium plates subjected to high velocity projectile impact, Mater. Des. 52 (2013) 1–16, https://doi.org/10.1016/j.matdes.2013.05.060.
[15] Y.A. Bahei-El-Din, G.J. Dvorak, Enhancement of blast resistance of sandwich plates, Compos. Part B Eng. 39 (2008) 120–127, https://doi.org/10.1016/j.compositesb.2007.02.006.
[16] M. Grujicic, B. Pandurangan, T. He, B. Cheeseman, C.-F. Yen, C.L. Randow, Computational investigation of impact energy absorption capability of polyurea coatings via deformation-induced glass transition, Mater. Sci. Eng., A 527 (2010) 7741–7751, https://doi.org/10.1016/j.msea.2010.08.042.

[17] H.M.C.C. Somarathna, S.N. Raman, A.A. Mutalib, K.H. Badri, Analysis of strain rate dependent tensile behaviour of polyurethanes, in: Proc. Int. Conf. Struct. Eng. Constr. Manag., Kandy, Sri Lanka, 2015, p. 7. https://scholar.google.com/citations?user=D0UxtzwAAAAJ&hl=en#d=gs_md_cita-d&p=&u=%2Fcitations%3Fview_op%3Dview_citation%26hl%3Den%26user%3DD0UxtzwAAAAJ%26citation_for_view%3DD0UxtzwAAAAJ%3A2osOgNQ5qMEC%26tzom%3D-330.
[18] H.M.C.C. Somarathna, S.N. Raman, A.A. Mutalib, K.H. Badri, Tensile behavior of polyurethane under low to intermediate strain rates (accessed May 31, 2016) Selangor, Malaysia, in: 13th Int. Conf. Concr. Eng. Technol., 2016, p. 6. https://scholar.google.com/citations?user=D0UxtzwAAAAJ&hl=en&gmla=AJsN-F5W8aPRw2Rt3506t2AqMBMOzlDw_gVrVlIDnkleclI7_dX9QAlPy17hwfugkFekqmxY5kAPeTTfKGVF__U6JhD3Y23eCD1ujTMdHW8aPmT-HnWWLXg&sciund=13986227814730560614#d=gs_md_cita-d&p=&u=%2Fcitations%3Fview_o.
[19] M.F. Omar, H.M. Akil, Z.A. Ahmad, Measurement and prediction of compressive properties of polymers at high strain rate loading, Mater. Des. 32 (2011) 4207–4215, https://doi.org/10.1016/j.matdes.2011.04.037.
[20] N.K. Naik, P.J. Shankar, V.R. Kavala, G. Ravikumar, J.R. Pothnis, H. Arya, High strain rate mechanical behavior of epoxy under compressive loading: Experimental and modeling studies, Mater. Sci. Eng., A 528 (2011) 846–854, https://doi.org/10.1016/j.msea.2010.10.099.
[21] G. Ravikumar, J.R. Pothnis, M. Joshi, K. Akella, S. Kumar, N.K. Naik, Analytical and experimental studies on mechanical behavior of composites under high strain rate compressive loading, Mater. Des. 44 (2013) 246–255, https://doi.org/10.1016/j.matdes.2012.07.040.
[22] S.N. Raman, T. Ngo, J. Lu, P. Mendis, Experimental investigation on the tensile behavior of polyurea at high strain rates, Mater. Des. 50 (2013) 124–129, https://doi.org/10.1016/j.matdes.2013.02.063.
[23] D. Mohotti, M. Ali, T. Ngo, J. Lu, P. Mendis, Strain rate dependent constitutive model for predicting the material behaviour of polyurea under high strain rate tensile loading, Mater. Des. 53 (2014) 830–837, https://doi.org/10.1016/j.matdes.2013.07.020.
[24] Y. Bai, C. Liu, G. Huang, W. Li, S. Feng, A hyper-viscoelastic constitutive model for polyurea under uniaxial compressive loading, Polymers (Basel). 8 (2016) 133, https://doi.org/10.3390/polym8040133.
[25] Z. Jia, G. Yuan, X. Feng, Y. Zou, Numerical study on the mechanical behavior of a polyurethane adhesive under high strain rate, Compos. Part B Eng. 158 (2019) 131–140, https://doi.org/10.1016/J.COMPOSITESB.2018.08.110.
[26] S.N. Raman, T. Ngo, P. Mendis, A review on the use of polymeric coatings for retrofitting of structural elements against, Blast Effects (2011).
[27] S.S. Sarva, S. Deschanel, M.C. Boyce, W. Chen, Stress e strain behavior of a polyurea and a polyurethane from low to high strain rates, 48 (2007) 2208–2213. doi:10.1016/j.polymer.2007.02.058.
[28] L. Bartolomé, J. Aurrekoetxea, M.A. Urchegui, W. Tato, The influences of deformation state and experimental conditions on inelastic behaviour of an extruded thermoplastic polyurethane elastomer, Mater. Des. 49 (2013) 974–980, https://doi.org/10.1016/j.matdes.2013.02.055.
[29] J.T. Fan, J. Weerheijm, L.J. Sluys, Compressive response of multiple-particles-polymer systems at various strain rates, Polymers (United Kingdom) 91 (2016) 62–73, https://doi.org/10.1016/j.polymer.2016.03.041.
[30] J.T. Fan, J. Weerheijm, L.J. Sluys, High-strain-rate tensile mechanical response of a polyurethane elastomeric material, Polymers (United Kingdom) 65 (2015) 72–80, https://doi.org/10.1016/j.polymer.2015.03.046.
[31] M.S.H. Fatt, I. Bekar, High-speed testing and material modeling of unfilled styrene butadiene vulcanizates at impact rates, J. Mater. Sci. 39 (2004) 6885–6899, https://doi.org/10.1023/B:JMSC.0000047530.86758.b9.
[32] J. Shim, D. Mohr, Using split Hopkinson pressure bars to perform large strain compression tests on polyurea at low, intermediate and high strain rates, Int. J. Impact Eng. 36 (2009) 1116–1127, https://doi.org/10.1016/j.ijimpeng.2008.12.010.
[33] C.M. Roland, J.N. Twigg, Y. Vu, P.H. Mott, High strain rate mechanical behavior of polyurea, 48 (2007) 574–578. doi:10.1016/j.polymer.2006.11.051.
[34] M. Grujicic, T. He, B. Pandurangan, F.R. Svingala, G.S. Settles, M.J. Hargather, Experimental Characterization and Material-Model Development for Microphase-Segregated Polyurea : An Overview, 21 (2012) 2–16. doi:10.1007/s11665-011-9875-6.
[35] M. Grujicic, B. Pandurangan, B. d'Entremont, The role of adhesive in the ballistic/structural performance of ceramic/polymer–matrix composite hybrid armor, Mater. Des. 41 (2012) 380–393, https://doi.org/10.1016/j.matdes.2012.05.023.
[36] M. Grujicic, W.C. Bell, B. Pandurangan, Design and material selection guidelines and strategies for transparent armor systems, Mater. Des. 34 (2012) 808–819, https://doi.org/10.1016/j.matdes.2011.07.007.
[37] D.K.K. Chattopadhyay, K.V.S.N.V.S.N. Raju, Structural engineering of polyurethane coatings for high performance applications, Prog. Polym. Sci. 32 (2007) 352–418, https://doi.org/10.1016/j.progpolymsci.2006.05.003.
[38] C.P. Buckley, C. Prisacariu, C. Martin, Elasticity and inelasticity of thermoplastic polyurethane elastomers: Sensitivity to chemical and physical structure, Polymer (Guildf) 51 (2010) 3213–3224, https://doi.org/10.1016/j.polymer.2010.04.069.
[39] R. Bonart, Thermoplastic Elastomers, Encycl. Polym, Sci. Technol. 20 (1979) 1389–1403, https://doi.org/10.1002/0471440264.pst105.
[40] H.F.F. Enderle, H.G.G. Kilian, B. Heise, J. Mayer, H. Hespe, Irreversible deformation of semicrystalline PUR-elastomers -a novel concept, Colloid Polym. Sci. 264 (1986) 305–322, https://doi.org/10.1007/BF01418190.
[41] F. Yeh, B.S. Hsiao, B.B. Sauer, S. Michel, H.W. Siesler, In-Situ Studies of Structure Development during Deformation of a Segmented Poly (urethane – urea) Elastomer, 2003, pp. 1940–1954.
[42] M. Mooney, A theory of large elastic deformation, J. Appl. Phys. 11 (1940) 582–592, https://doi.org/10.1063/1.1712836.
[43] R.S. Rivlin, Large elastic deformations of isotropic materials. IV. Further developments of the general theory, Philos. Trans. R. Soc. A Math. Phys. Eng. Sci. 241 (1948) 379–397, https://doi.org/10.1098/rsta.1948.0024.
[44] R.W. Ogden, Large,, Deformation isotropic elasticity: on the correlation of theory and experiment for compressible rubberlike solids, Proc. R. Soc. London A Math. Phys. Eng. Sci. 328 (1972) 567–583, https://doi.org/10.1098/rspa.1972.0096.
[45] T.D. Canonsburg, ANSYS Mechanical User ' s Guide, 15317 (2013) 724–746.
[46] J. Hallquist, LS-DYNA ® KEYWORD USER'S MANUAL VOLUME I, Livermore, California, 2007. www.lstc.com.
[47] C. Li, J. Lua, A hyper-viscoelastic constitutive model for polyurea, Mater. Lett. 63 (2009) 877–880, https://doi.org/10.1016/j.matlet.2009.01.055.
[48] V. Amirkhizi, J. Isaacs, J. McGee, S. Nemat-Nasser, An experimentally-based viscoelastic constitutive model for polyurea, including pressure and temperature effects, Philos. Mag. 86 (2006) 5847–5866, https://doi.org/10.1080/14786430600833198.
[49] D.S. Kleponis, An Analysis of Parameters for the Johnson-Cook Strength Model for 2-in-Thick Rolled Homogeneous Armor, Army Res. Lab. Aberdeen Proving Ground, MD 21005-5066. Weapons an (2001) 36.
[50] D. Forni, B. Chiaia, E. Cadoni, High strain rate response of S355 at high temperatures, Mater. Des. 94 (2016) 467–478, https://doi.org/10.1016/j.matdes.2015.12.160.
[51] K.H. Badri, S.H. Ahmad, S. Zakaria, Production of a High-Functionality RBD Palm Kernel Oil-Based Polyester Polyol, (2001) 384–389.
[52] K. Haji, Biobased polyurethane from palm kernel oil-based polyol, Polyurethane (2012) 447–470, https://doi.org/10.5772/47966.